Cell Reports

Article

Enforced activation of the CREB/KDM2B axis prevents alcohol-induced embryonic developmental delay

Graphical abstract

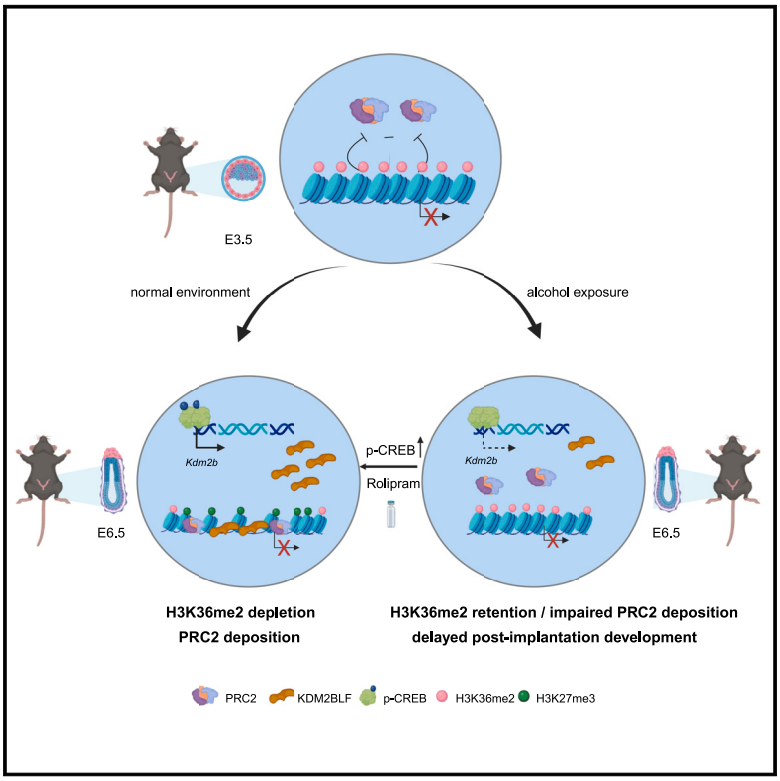

Highlights

- Peri-implantation embryos exposed to alcohol show development delay
- Inadequate KDM2BLF expression hinders H3K27me3 deposition at development regulator genes
- Acetaldehyde causes CREB inactivation and thereby fails to induce KDM2BLF expression
- Enhanced CREB activation mitigates developmental delays induced by alcohol exposure

Authors

Hang Liu, Qiyu Ren, Meihan Gong, ..., Xiaozhi Liu, Cailing Lu, Xudong Wu

Correspondence

lucailing@nrifp.org.cn (C.L.), wuxudong@tmu.edu.cn (X.W.)

In brief

Alcohol exposure during peri-implantation delays embryonic development. Liu et al. show that acetaldehyde-induced CREB inactivation reduces KDM2BLF expression, impairing H3K27me3 establishment at developmental regulator genes. PDE4 inhibitors, which activate CREB, offer a potential preventative approach against ethanol-induced developmental defects.

Liu et al., 2024, Cell Reports *43*, 115075
December 24, 2024
https://doi.org/10.1016/j.celrep.2024.115075

CellPress

Cell Reports

CellPress
OPEN ACCESS

Article

Enforced activation of the CREB/KDM2B axis prevents alcohol-induced embryonic developmental delay

Hang Liu,[1,5] Qiyu Ren,[2,5] Meihan Gong,[1,5] Feifei Zuo,[1] Qian Li,[1] Dawei Huo,[1,3] Ye Yuan,[1] Yutong Zhang,[2] Yu Kong,[1] Xiaozhi Liu,[4] Cailing Lu,[2,*] and Xudong Wu[1,4,6,*]

[1]State Key Laboratory of Experimental Hematology, the Province and Ministry Co-sponsored Collaborative Innovation Center for Medical Epigenetics, Key Laboratory of Immune Microenvironment and Disease (Ministry of Education), Tianjin Key Laboratory of Medical Epigenetics, Department of Cell Biology, Tianjin Medical University, Qixiangtai Road 22, Tianjin 300070, China

[2]Department of Genetics, National Research Institute for Family Planning, Chinese Academy of Medical Sciences & Peking Union Medical College, Beijing 100081, China

[3]Bone Marrow Transplantation Center, the First Affiliated Hospital, Zhejiang University School of Medicine, Liangzhu Laboratory, Institute of Hematology, Zhejiang University, Hangzhou 311113, China

[4]Tianjin Key Laboratory of Epigenetics for Organ Development of Premature Infants, Tianjin 300450, China

[5]These authors contributed equally

[6]Lead contact

*Correspondence: lucailing@nrifp.org.cn (C.L.), wuxudong@tmu.edu.cn (X.W.)

https://doi.org/10.1016/j.celrep.2024.115075

SUMMARY

Unintentional, early pregnancy alcohol consumption affects embryonic development. During the peri-implantation stage, coinciding with the transition from naive to primed pluripotency, the long isoform of KDM2B (KDM2BLF) underlies the *de novo* establishment of polycomb repressive complex (PRC) functions at promoters after fertilization. However, it remains unclear whether and how ethanol exposure affects this spatiotemporal chromatin setting. Here, we show that exposing peri-implantation mouse embryos to ethanol leads to impaired post-implantation development, mirrored by the delayed exit of naive pluripotency in acetaldehyde-treated embryonic stem cells. Remarkably, these abnormalities are linked to inadequate KDM2BLF expression and compromised deposition of PRC marks, which arise from cAMP response element-binding protein (CREB) inactivation. Accordingly, pharmacological activation of CREB effectively restores pluripotency transition partly dependent on KDM2BLF *in vitro* and ameliorates post-implantation embryonic defects *in vivo*. Therefore, our study highlights the pivotal role of the CREB/KDM2B axis in chromatin configuration and developmental programming, proposing potential preventive strategies against ethanol exposure-induced detrimental effects.

INTRODUCTION

In mammalian development, mothers transmit environmental cues, such as nutritional status, to embryos or the fetus through the placenta, with the peri-implantation period being particularly sensitive. Environmental exposures during this critical stage may exert profound effects on subsequent development and may even influence postnatal health. In mice, implantation of blastocyst begins on embryonic day (E)4.75–E5.0, followed by gastrulation and the formation of three germ layers. These development programs depend not only on genetic information but also on the spatiotemporally coordinated chromatin states, known as epigenetic information. Environmental exposures predominantly impose complex epigenetic influences on developmental processes.

Polycomb group (PcG) proteins, as highly conserved epigenetic regulators, play crucial roles in lineage specification.[1,2] Mouse genetic studies have demonstrated that the loss of core PcG members results in gastrulation arrest.[3–6] However, the impact of environmental factors on PcG functions is not well understood. Biochemically, PcG proteins form multi-protein complexes that maintain target genes in a transcription repression state. These complexes, known as polycomb repressive complexes (PRCs), exert their biophysical or biochemical activities on chromatin. For instance, PRC2 catalyzes H3K27 tri-methylation (H3K27me3) mainly at CpG-rich regions, known as CpG islands (CGIs).[1,2] In mouse, H3K27me3 enrichment commences at the CGI promoters of developmental regulator genes during embryonic implantation.[7,8] Similar dynamic epigenomic profiles of H3K27me3 are mirrored in the *in-vitro*-cultured mouse embryonic stem cells (mESCs), transitioning from naive (MEK and GSK3β inhibitors plus LIF [2iL]) to intermediate (serum plus LIF [SL]) and primed pluripotent states (FGF2 plus Activin [FA]).[9–12] This spatiotemporal establishment of PRC2 functions at

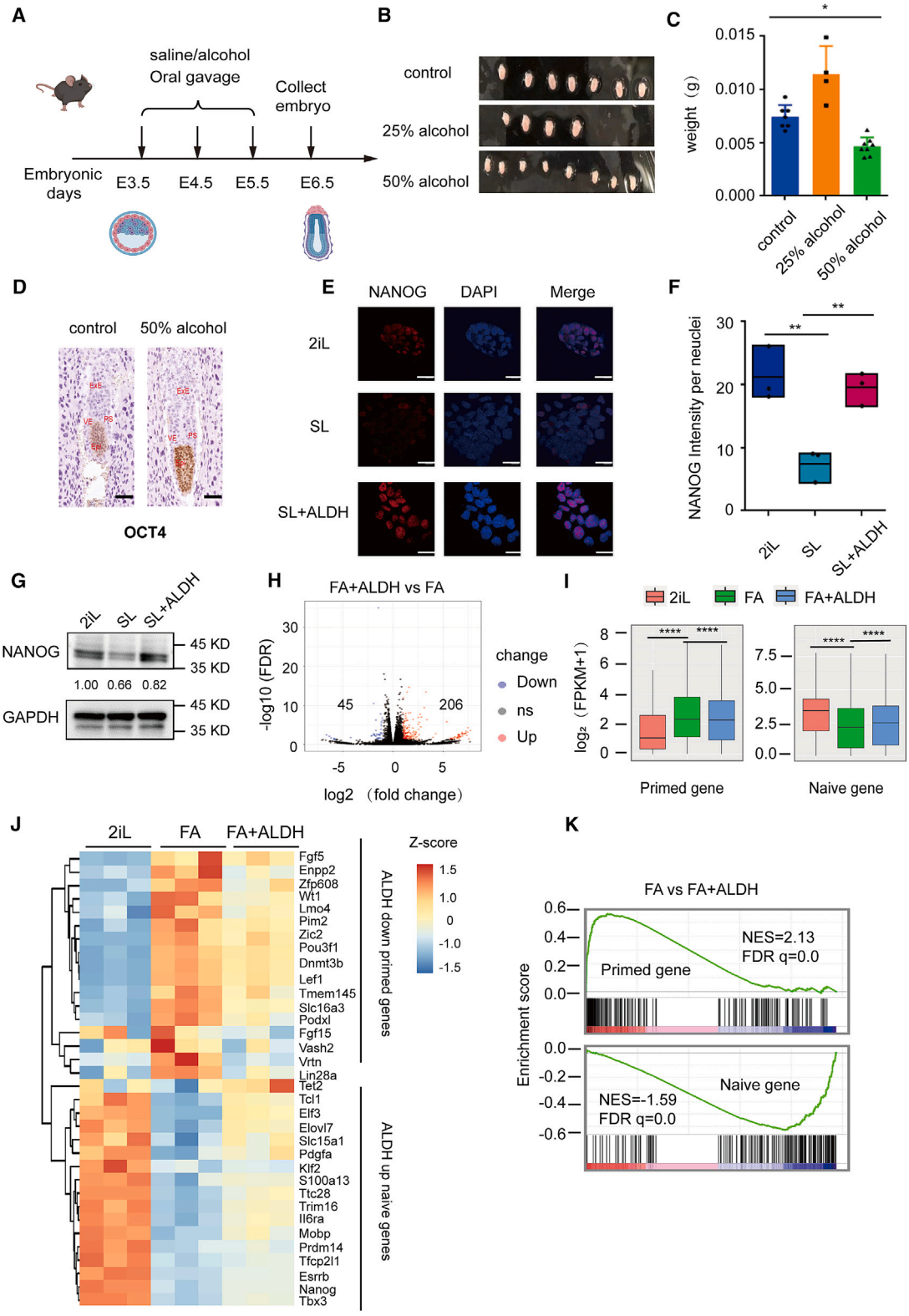

Figure 1. Exposure of peri-implantation embryos to ethanol causes delayed post-implantation development

(A) Scheme of mouse models with ethanol exposure at peri-implantation stage. Saline or varying concentrations of alcohol were administrated by oral gavage at specified time points, and embryos were collected at E6.5.

(legend continued on next page)

promoters is essential for priming development regulator genes for transcriptional responses to differentiation cues throughout the following embryonic development.[2,13,14]

In a previous study, we identified the long isoform of KDM2B (KDM2BLF) as the molecular basis for the *de novo* establishment of PRC2 at the CGI promoters during embryonic development.[15] As a chromatin regulator with pleiotropic functions, KDM2B binds unmethylated CpG-rich DNA sequences through its CXXC structural domain, forms PRC1 to catalyze H2AK119 monoubiquitylation (H2AK119ub1),[16] and removes H3K36me2 marks through its JmjC domain.[17] The H3K36me2 demethylase activity is specific to KDM2BLF, which is selectively transcribed from an alternative promoter from the short isoform (SF) at the peri-implantation stage and reconfigures CGI promoters for PRC establishment at promoters.[15,18] KDM2BLF deficiency detrimentally impacts the exit from naive pluripotency *in vitro* and leads to embryonic developmental arrest post-implantation.[15] However, the mechanisms governing the spatiotemporal induction of KDM2BLF expression during the peri-implantation stage remain unclear.

Alcohol, an easily accessible teratogen, crosses the placenta and can damage the developing neural, cardiac, and endocrine systems.[19–22] Accumulating evidence has demonstrated that ethanol exposure induces epigenetics changes, including histone acetylation, histone methylation, and DNA methylation alterations, linking to embryo malformation.[23–26] Nevertheless, a definitive causal relationship between ethanol-induced epigenetic aberration and embryo developmental defects has yet to be established. Since unintentional alcohol consumption often occurs in early pregnancy, we wonder whether it may impair the peri-implantation PRC establishment at promoters, thereby delaying post-implantation embryonic development.

In this study, we find that activated CREB (cAMP response element-binding protein) orchestrates the induction of KDM2BLF expression during the exit from naive pluripotency. We also show that peri-implantation ethanol exposure causes post-implantation developmental defects, accompanied by diminished KDM2BLF expression and impaired PRC2 establishment at the promoter in epiblasts. These defects, arising from CREB inactivation, can be mitigated by constitutively active CREB (caCREB) or the phosphodiesterase type 4 (PDE4) inhibitor rolipram, both of which activate CREB and enhance downstream KDM2BLF expression. Moreover, rolipram restores the developmental program partly dependent on KDM2BLF. Thus, our findings underscore the pivotal roles of the CREB/KDM2B axis in shaping chromatin architecture and orchestrating developmental processes, offering promising strategies for preventing the adverse effects of ethanol exposure during early pregnancy.

RESULTS

Ethanol exposure leads to post-implantation embryonic developmental defects through ALDH

To assess the impact of ethanol exposure on early embryogenesis, we established a mouse model involving peri-implantation embryos. Pregnant mice were administered either saline or alcohol at a concentration of 25% or 50% via gavage at an approximate dosage of 10 μL per gram of body weight[27,28] on E3.5, E4.5, and E5.5, with embryo analysis conducted on E6.5 (Figure 1A). Compared to the control group, both embryo sizes and weights significantly decreased after alcohol treatment (Figures 1B and 1C). Immunohistochemical (IHC) staining of E6.5 epiblasts revealed a notable retention of OCT4-positive cells in the alcohol-treated group (Figure 1D), indicating a delayed exit from naive pluripotency. These data imply that exposing peri-implantation embryos to ethanol causes post-implantation developmental delays.

Given that ethanol is metabolized to acetaldehyde (ALDH) and acetic acid *in vivo*, we explored which of these metabolites may contribute to the post-implantation developmental delay. *In-vitro*-cultured mESCs were treated with ethanol, ALDH, or acetic acid as they transitioned from 2iL to SL culture conditions. In the control group, the expression levels of NANOG, a marker of naive pluripotency, are significantly downregulated upon the switch, as confirmed by quantitative reverse-transcription PCR (RT-qPCR), western blot (WB), or immunofluorescence (IF) analyses. Intriguingly, the decrease of NANOG expression levels is not affected by gradient concentrations of ethanol or acetic

(B) Morphological comparison of mouse E6.5 embryos in control and ethanol-treated groups.
(C) Weight of mouse E6.5 embryos in control and ethanol-treated groups. Control group: $n = 9$, 25% alcohol: $n = 5$, 50% alcohol: $n = 8$.
(D) Representative immunostaining of OCT4 in E6.5 embryos in control and ethanol-treated groups. The staining was performed in three embryos from each group.
(E) IF analysis of NANOG in mESCs cultured under 2iL, SL, and SL+ALDH conditions. Scale bars, 100 μm.
(F) Boxplots display quantitative fluorescence analysis using CellProfiler software. At least 50 nuclei of treated or control cells from triplicate experiments were used to quantify the NANOG intensities, and the p values were determined by Student's t test.
(G) WB analysis of NANOG levels with GAPDH as loading control.
(H) Volcano plot of DEGs in FA-mESCs treated or untreated with ALDH. DEGs were selected by fold change >1.5 ($p < 0.05$). The x axis shows the $\log_2$ (fold change) in gene expression between FA+ALDH and FA group, and the y axis shows the statistical significance of the differences. Splashes with different colors represent different groups of genes as indicated in the bottom right corner. RNA-seq data are from biological triplicates.
(I) Boxplots showing $\log_2$-transformed expression levels of naive and primed pluripotency genes in the three treatment groups. The boxplots indicate that the median (center line) p value of comparison was determined by two-sided unpaired t test. ****$p < 0.0001$.
(J) Heatmap showing the relative expression levels of naive and primed pluripotency genes in mESCs cultured under 2iL, FA, and FA+ALDH conditions. Gene expression levels are shown as relative Z scores across the samples.
(K) GSEA analysis of naive and primed pluripotency genes in the three treatment groups. Gene lists are defined by GEO: GSE145727.[29] NES, normalized enrichment score. False discovery rate (FDR) q = 0.
(C and F) Data are represented as means ± SEM. Statistical tests were performed using two-tailed unpaired t test with Welch's correction. *$p < 0.05$ and **$p < 0.01$.
See also Figures S1 and S2 and Table S1.

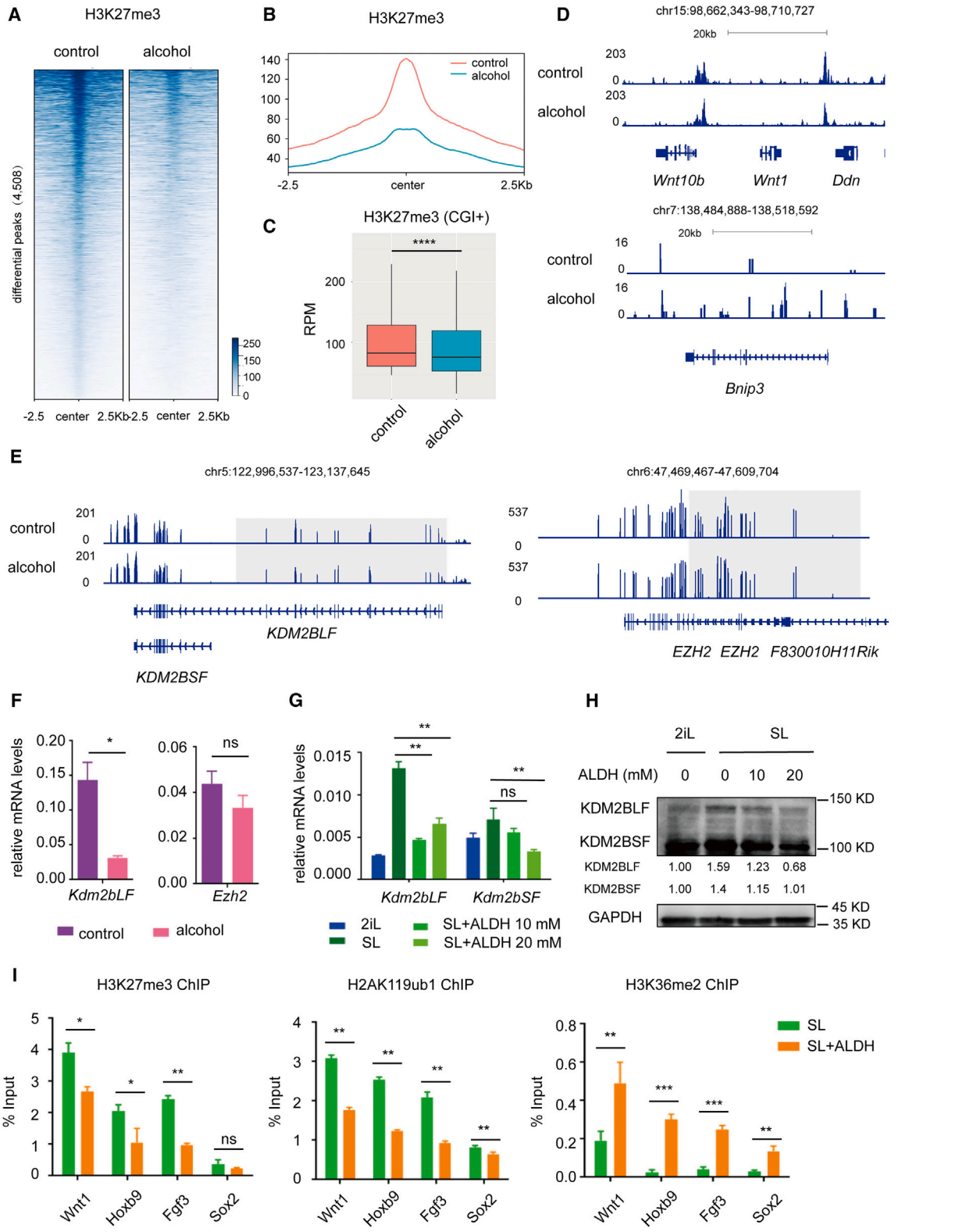

(legend on next page)

acid but is significantly reversed by ALDH treatment (10–20 mM; detailed in experimental model) (Figures S1A, S1B, and 1E–1G). Actually, increasing the concentration of acetic acid even expedites mESC differentiation, as observed from the morphological changes (Figure S1C), despite elevating global histone acetylation levels (Figure S1D). In contrast, alkaline phosphatase (AP) staining analysis showed that ALDH treatment results in a significantly increased number of compact and round colonies with high AP activity (Figure S2A). Thus, the ALDH-induced hyper-naive pluripotent state mimics the delayed development in embryos.

For a more comprehensive understanding of ALDH-induced molecular alterations, we performed RNA sequencing (RNA-seq) analysis in mESCs cultured under 2iL, FA, or FA+ALDH conditions. Among the differentially expressed genes (DEGs) by ALDH in FA conditions (Table S1; Figure 1H), those downregulated (45 genes) are significantly enriched in neurogenesis, gliogenesis, neuroepithelial cell differentiation, etc. (Figure S2B), suggesting that ALDH impairs the neuroectoderm development potential at the primed pluripotent state. Focusing on the pluripotency transcriptional programs, we confirmed that the expression levels of naive marker genes are downregulated, while the expression levels of primed genes are upregulated upon switching from 2iL to FA in the control group. Notably, this transition from naive to primed transcriptional programs is significantly disrupted by ALDH treatment (Table S1; Figures 1I and 1J). Gene set enrichment analysis (GSEA) reveals a significant enrichment of naive gene signatures in the FA+ALDH group, in stark contrast to the pronounced enrichment of primed gene signatures observed in the FA group (Figure 1K). Moreover, the reversing effects on the dynamic expression changes of representative pluripotency genes were validated by RT-qPCR analyses (Figure S2C). These data indicate that ALDH treatment delays the exit from naive pluripotency, contributing to the retardation of post-implantation embryonic development.

Ethanol exposure impedes post-implantation PRC2 establishment at promoters through ALDH-impaired KDM2BLF expression and activity

Given the crucial roles of PRC establishment in post-implantation embryonic development, we sought to investigate whether the peri-implantation ethanol exposure affects H3K27me3 deposition in post-implantation embryos. Accordingly, we isolated the E6.5 epiblasts from the ethanol-exposed mouse embryos and subjected them to cleavage under targets and tagmentation (CUT&Tag) analysis. The comparative analysis revealed a striking disruption of H3K27me3 deposition in embryos exposed to 50% alcohol compared to the control group (Table S2; Figures 2A and 2B). The significance of the H3K27me3 intensity decrease at CGI promoters is illustrated in Figure 2C, and this effect is exemplified by the genomic view at conventional PcG target genes, with non-PcG target genes serving as a negative control (Figure 2D). Gene Ontology (GO) analyses of these H3K27me3-deficient genes show that their functions are mainly associated with pattern specification processes, regionalization, and the development of the nervous and skeletal systems, among others (Figure S3A). These data indicate that alcohol exposure leads to an almost non-discriminatory impairment of H3K27me3 deposition at development regulator genes. This epigenomic deficiency is consistent with the delayed exit from naive pluripotency as evidenced by transcriptomic changes.

Considering that KDM2BLF readies CGI promoters for PRC2 nucleation,[15] we proceeded to find out whether these epigenomic and phenotypic aberrations are attributable to compromised KDM2BLF expression in alcohol-exposed embryos. As compared through RNA-seq and RT-qPCR analyses in epiblasts, KDM2BLF mRNA levels are decreased in the group of alcohol-exposed embryos compared to the control, while the expression levels of H3K27me3 regulators EZH1/2 and KDM6A/B remain unchanged (Figures 2E, 2F, and S3B). Consistently, the treatment of 10 or 20 mM ALDH in SL-mESCs results in a striking decrease of KDM2BLF expression levels together with a minor decrease of KDM2BSF levels (Figures 2G and 2H). Consistently, chromatin immunoprecipitation (ChIP)-qPCR analysis confirmed an inadequate depletion of H3K36me2 and insufficient deposition of H3K27me3 and H2AK119ub1 at PcG target gene promoters in 20 mM ALDH-treated mESCs (Figure 2I). Therefore, the insufficient post-implantation PRC establishment at promoters subsequent to ethanol exposure is attributable to impaired KDM2BLF expression and demethylase activity by ALDH.

Figure 2. Ethanol exposure impedes post-implantation PRC2 establishment at promoters through ALDH-impaired KDM2BLF expression and activity

(A) Heatmap showing the differential H3K27me3 signals identified by MACS2 bdgdiff with the default settings in control and alcohol-treated E6.5 epiblasts ($n = 2$ for each group). Colors represent CUT&Tag reads per million (RPM), and rows are ranked by the signals in control group.

(B) Line charts showing the average differential H3K27me3 signals in (A). The x axis represents the distance to peak center.

(C) Boxplots comparing H3K27me3 signals at CGI promoters in control and alcohol-treated E6.5 epiblasts. The boxplots indicate the median (center line), the third and first quartiles (box limits), and 1.5× interquartile range (IQR) above and below the box (whiskers). Data are represented as means ± SEM. p value of comparison was determined by two-sided unpaired t test. ****$p < 0.0001$.

(D) The IGV view of H3K27me3 enrichment in control and alcohol-treated epiblasts at H3K27me3-positive-CGIs (up) and H3K27me3-negative regions (below). Signals represent RPM.

(E and F) The IGV view and RT-qPCR analysis of KDM2B and EZH2 mRNA levels in control and alcohol-treated epiblasts.

(G and H) RT-qPCR and WB analysis of KDM2BLF and KDM2BSF expression in 2iL-, SL-, or SL+ALDH-mESCs. GAPDH serves as the loading control in (H).

(I) ChIP-qPCR analysis comparing enrichment of designated histone marks at PcG target gene promoters and active promoters in control and ALDH-treated mESCs.

Data are represented as means ± SEM. Statistical tests were performed using two-tailed unpaired t test with Welch's correction in (F), (G), and (I). $n \geq 3$, *$p < 0.05$ and **$p < 0.01$, n.s., nonsignificant.

See also Figure S3 and Table S2.

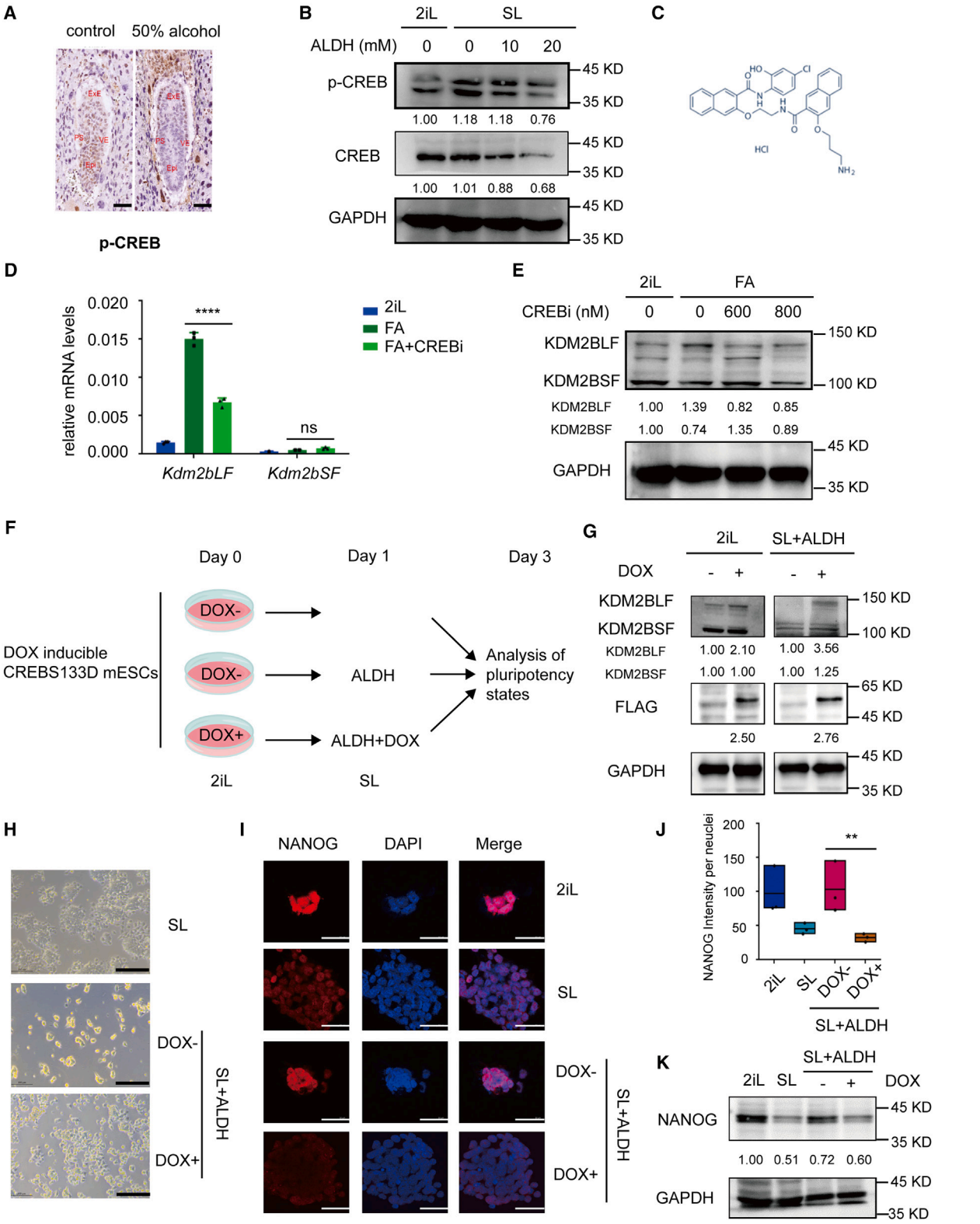

Figure 3. Impaired KDM2BLF induction and pluripotency transition by ALDH treatment are attributed to CREB inactivation

(A) Representative IHC images of p-CREB levels in E6.5 embryos from the control and alcohol-treated groups. The IHC assay was performed in three embryos from each group.

(legend continued on next page)

Impaired KDM2BLF induction by ALDH treatment is attributed to CREB inactivation

To unravel the mechanisms underlying the impaired transcriptional induction of KDM2BLF by ALDH treatment, we sought to identify the upstream regulatory factors involved. Intriguingly, previous reports indicate that fibroblast growth factor (FGF) signaling-activated CREB upregulates KDM2B expression in cancer cells,[30] and FGF-MAPK signaling is activated during pluripotency exit, phosphorylating CREB at serine 133 for downstream transcription induction[31,32] (Figure S4A). Thus, we proceeded to examine the kinetics of CREB expression and activity.

Upon switching the culture medium from 2iL to SL to FA, a continuous increase in total CREB expression and phosphorylation (p-CREB) levels was observed (Figure S4B). Consistently, ChIP-qPCR analysis showed that p-CREB enrichment at the transcription start site (TSS) of *Kdm2bLF*, but not *Kdm2bSF*, is significantly increased in SL-mESCs compared with that in 2iL-mESCs (Figure S4C). Furthermore, when CREB is depleted in mESCs through lentivirally expressed short hairpin RNAs (shRNAs), KDM2BLF expression is significantly reduced at both mRNA and protein levels, while KDM2BSF expression remains unchanged (Figures S4D and S4E). These data indicate a direct and specific transcription regulation of KDM2BLF by activated CREB.

Then, we investigated whether ALDH treatment leads to CREB inactivation. IHC staining of E6.5 epiblasts revealed significantly lower p-CREB levels in ethanol-treated embryos compared to the control group. Likewise, ALDH treatment in SL-mESCs results in a dose-dependent decrease in total and phosphorylated CREB levels (Figures 3A and 3B). Moreover, when we treated FA-mESCs with a CREB inhibitor, a significant downregulation of KDM2BLF expression was observed (Figures 3C–3E). Thus, activated CREB during pluripotency transition induces KDM2BLF expression, which is impaired by ALDH treatment.

Impaired pluripotency transition by ALDH treatment is attributed to CREB inactivation

Notably, *Creb* deletion in mouse embryos results in early developmental defects.[33] Thus, we examined how CREB deficiency in mESCs might affect the exit from naive pluripotency. Comparative analysis via AP staining revealed a substantial reversal of decreased AP activity in FA-mESCs upon CREB depletion or inhibition (Figures S5A and S5B). IF analysis showed that NANOG remains homogenously expressed in CREB-inhibited FA-mESCs, like in 2iL-mESCs (Figures S5C and S5D). Furthermore, RT-qPCR analysis demonstrated that CREB inhibition significantly impedes the upregulation or downregulation of representative pluripotency marker gene expression in FA-mESCs (Figure S5E). Collectively, these data indicate an indispensable role of CREB activity in the exit from naive pluripotency.

Nevertheless, a variety of factors may account for ALDH-delayed pluripotency transition. To substantiate the causal effect of CREB inactivation, we engineered an ESC line with an inducible expression of caCREB (icaCREB) (Figure 3F), similar to our previous generation of inducible CRISPRi/a systems.[34,35] The FLAG-tagged CREBS133D was inserted downstream of the tetracycline-responsive element (TRE) promoter in an A2LoxCre ESC[35] (Figures S6A and S6B; details in experimental model). Upon 24 h of doxycycline (DOX) treatment, caCREB expression is strikingly induced, accompanied by a significant upregulation of KDM2BLF expression under 2iL culture conditions. More importantly, DOX-induced caCREB rescues the diminished KDM2BLF expression in SL+ALDH mESCs (Figure 3G). These data strongly support CREB as an upstream activator for KDM2BLF expression.

Subsequently, we analyzed the pluripotent states in these cells (Figure 3F). Comparative analysis of cell morphology and NANOG expression levels indicated a significant reversal of the ALDH-induced delay during exit from naive pluripotency following DOX addition (Figures 3H–3K). These data suggest that artificially activated CREB is sufficient to rescue the negative impact of ALDH on pluripotency transition.

Rolipram rescues ALDH-impeded PRC establishment at promoters and pluripotency transition through KDM2BLF

To chemically rescue the developmental program, we endeavored to identify a direct agonist of CREB or a modulator to indirectly activate CREB. Given the absence of a specific agonist, we turned to cAMP-specific PDE4 inhibitors, known to elevate cAMP levels, thereby activating downstream cascades, including CREB.[36,37] (Figure S7A) These inhibitors, with rolipram as a notable example, have a history of clinical use as anti-inflammatory medications and are known for their favorable safety

(B) WB analysis comparing p-CREB levels in 2iL-, SL-, or SL+ALDH-mESCs.
(C) The structural formula of CREB inhibitor (CREBi) 666-15.
(D) RT-qPCR analysis of KDM2B expression levels in 2iL-, FA-, or FA+CREBi-mESCs. Data are represented as means ± SEM. Two-tailed unpaired t test. $n = 3$, $^{****}p < 0.0001$, n.s., nonsignificant.
(E) WB analysis comparing KDM2B expression levels in 2iL-, FA-, or FA+CREBi-mESCs.
(F) Experimental flow pattern diagram: culture conditions of DOX-inducible CREBS133D mESCs (icaCREB) were switched from 2i/L to SL with or without ALDH treatment. Pluripotent states were compared after 2 days.
(G) WB analysis showing the expression of FLAG-CREBS133D, KDM2BLF and KDM2BSF in designated groups of cells.
(H) Morphology of icaCREB-mESCs in SL or SL+ALDH conditions with or without DOX. Scale bars, 100 μm.
(I) IF analysis comparing NANOG expression levels in icaCREB-mESCs among the designated groups. Scale bars, 100 μm.
(J) Quantitative analysis of NANOG signals was performed using CellProfiler software. At least 50 nuclei of treated or control cells from triplicate experiments were used to quantify the NANOG intensities. Data are represented as means ± SEM. Statistical tests were performed using two-tailed unpaired t test with Welch's correction. $^{**}p < 0.01$.
(K) WB analysis of NANOG levels with GAPDH as loading control.
GAPDH serves as the loading control in (B), (E), and (G).
See also Figures S4–S6.

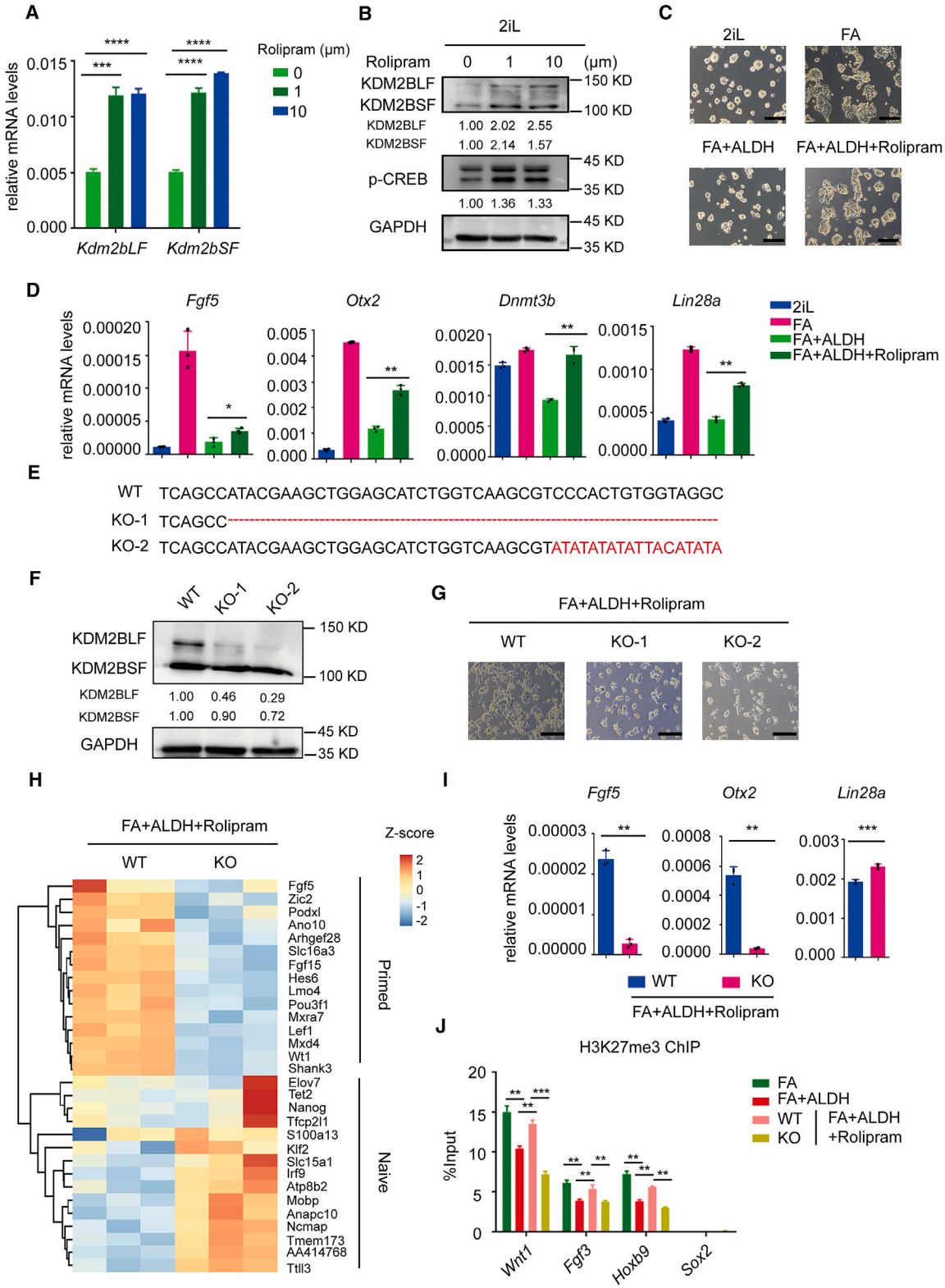

Figure 4. Rolipram restores pluripotency transition following ALDH treatment in a KDM2BLF-dependent manner

(A) RT-qPCR analysis comparing the levels of KDM2BLF and SF in mESCs with or without rolipram.

(B) WB analysis showing the levels of KDM2BLF, KDM2BSF, and p-CREB in mESCs with or without rolipram.

(legend continued on next page)

records. Rolipram was chosen for its potential to cross the blood-placenta barrier, given its past testing as an antidepressant that can permeate the blood-brain barrier.[38]

As expected, rolipram induces CREB phosphorylation and upregulates KDM2BLF and SF expression levels in mESCs (Figures 4A and 4B). Similar to the caCREB induction, rolipram modestly but significantly restores cell flattening and primed pluripotency marker gene expression in the presence of ALDH (Figures 4C and 4D). When *Kdm2bLF* is specifically deleted (knockout [KO]) (Figures 4E and 4F), CREB expression and its phosphorylation are modestly compromised (Figures S7B and S7C), indicating a potential functional interplay even though CREB acts upstream of *Kdm2b*.

Notably, rolipram fails to restore the morphological flattening in *Kdm2bLF*-KO mESCs as observed in wild type (WT) (Figure 4G). To quantitatively assess transcriptional programs, we conducted transcriptomic analysis to compare the pluripotent states in KO and WT mESCs in the presence of ALDH and rolipram. Focusing on the DEGs, we found that rolipram significantly restores the upregulation of primed marker genes and the downregulation of naive marker genes in ALDH-treated WT cells, while the restoration of a subset of genes is less effective in KO cells (Figures 4H and 4I). Moreover, ChIP-qPCR analysis showed that the insufficient H3K27me3 deposition at representative PcG target gene promoters is significantly rescued by rolipram in ALDH-treated WT cells but not KO cells (Figure 4J). Together, these data indicate that rolipram rescues ALDH-impaired pluripotency transition and the inadequate PRC establishment at promoters partly dependent on KDM2BLF.

Rolipram potentiates CREB activity and alleviates the post-implantation developmental defects caused by ethanol exposure

To further assess whether rolipram mitigates the ethanol-induced post-implantation developmental defects, we administered rolipram via intraperitoneal injection in the established mouse model of peri-implantation ethanol exposure (Figure 5A). Upon harvesting embryos at E6.5, we observed a significant reversal of the decrease in embryo volumes and weights induced by 50% ethanol exposure due to rolipram treatment (Figures 5B and 5C). IHC analysis shows that rolipram prevents the decrease of CREB activity and retention of OCT4-positive cells caused by ethanol exposure (Figures 5D and 5E). Furthermore, we isolated epiblasts from the different experimental groups for RNA-seq analysis (DEGs shown in Table S3). Focusing on the representative naive and primed pluripotency marker genes, we found that rolipram significantly reverses the upregulated expression of primed marker genes and the downregulation of naive marker genes in alcohol-exposed embryos (Figure 5F). These data confirm that rolipram successfully mitigates the developmental defects caused by peri-implantation alcohol exposure.

DISCUSSION

Despite significant advances in epigenetic studies, direct links between adverse environmental influences and dysregulated chromatin landscapes have yet to be firmly established. The roles of epigenetic adaptation to environmental exposures in developmental plasticity have emerged recently.[39] In this study, we employ both peri-implantation embryo and pluripotency transition models to elucidate the consequences and epigenetic rewiring resulting from acute ethanol exposure. Our findings reveal that ethanol/ALDH exposure disrupts CREB-mediated KDM2BLF expression, leading to impaired transcriptional programs and PRC establishment at promoters. Moreover, enforced activation of CREB signaling can rectify delays in exiting naive pluripotency and developmental delay. As a proof of concept, the use of rolipram has been shown to effectively reverse alcohol-induced developmental defects, specifically through a KDM2BLF-dependent epigenetic resetting (Figure 6).

The teratogenic effects of alcohol on developing embryo and postnatal individuals are collectively termed as fetal alcohol spectrum disorders (FASDs).[23,40] So far, no molecular markers have been established for the detection of FASDs and their associated risks. *In utero* ethanol exposure has been shown to result in significant epigenetic changes, for example, global DNA hypomethylation.[26,41,42] In addition, alcohol metabolism in the liver leads to a rapid increase in blood acetate concentration and, therefore, the elevation of protein acetylation levels.[43] Consistently, prenatal alcohol exposure has been found to cause altered histone acetylation in mouse embryos,[27,41,44–46] though our data show that increased histone acetylation in ESCs following acetate treatment does not affect the exit from naive pluripotency. While ALDH has been recognized for its diverse cytotoxic effects on various cell types,[47] its significance in epigenetic dysregulation has remained unclear. Our current study sheds light on the impaired PRC establishment at promoters by ALDH during a brief time frame of pluripotency transition. Nevertheless, comprehensive investigations are warranted to assess potential genome instability and other epigenome-wide changes.

(C) Morphology of mESCs cultured under 2iL, FA, FA+ALDH, or FA+ALDH+rolipram conditions.
(D) RT-qPCR analysis of primed pluripotency gene in mESCs cultured under indicated conditions.
(E) Sanger sequencing analysis confirming two CRSIPR-Cas9-edited *Kdm2bLF* KO subclones.
(F) WB analysis confirming the depletion of KDM2BLF expression.
(G) Morphology of WT or *Kdm2bLF*-KO mESCs in indicated conditions.
(H) Heatmap showing the relative expression of naive and primed pluripotency genes in WT and *Kdm2bLF*-KO mESCs under FA+ALDH+rolipram conditions for 24 h.
(I) RT-qPCR analysis of primed pluripotency gene WT or *Kdm2bLF*-KO mESCs under FA+ALDH+rolipram conditions.
(J) ChIP-qPCR analysis of H3K27me3 in WT and *Kdm2bLF*-KO cells cultured under indicated conditions.
GAPDH serves as the loading control in (B) and (F). Data are represented as means ± SEM. Two-tailed unpaired t test was used for (A), (D), (I), and (J). $*p < 0.05$, $**p < 0.01$, and $***p < 0.001$.
See also Figure S7.

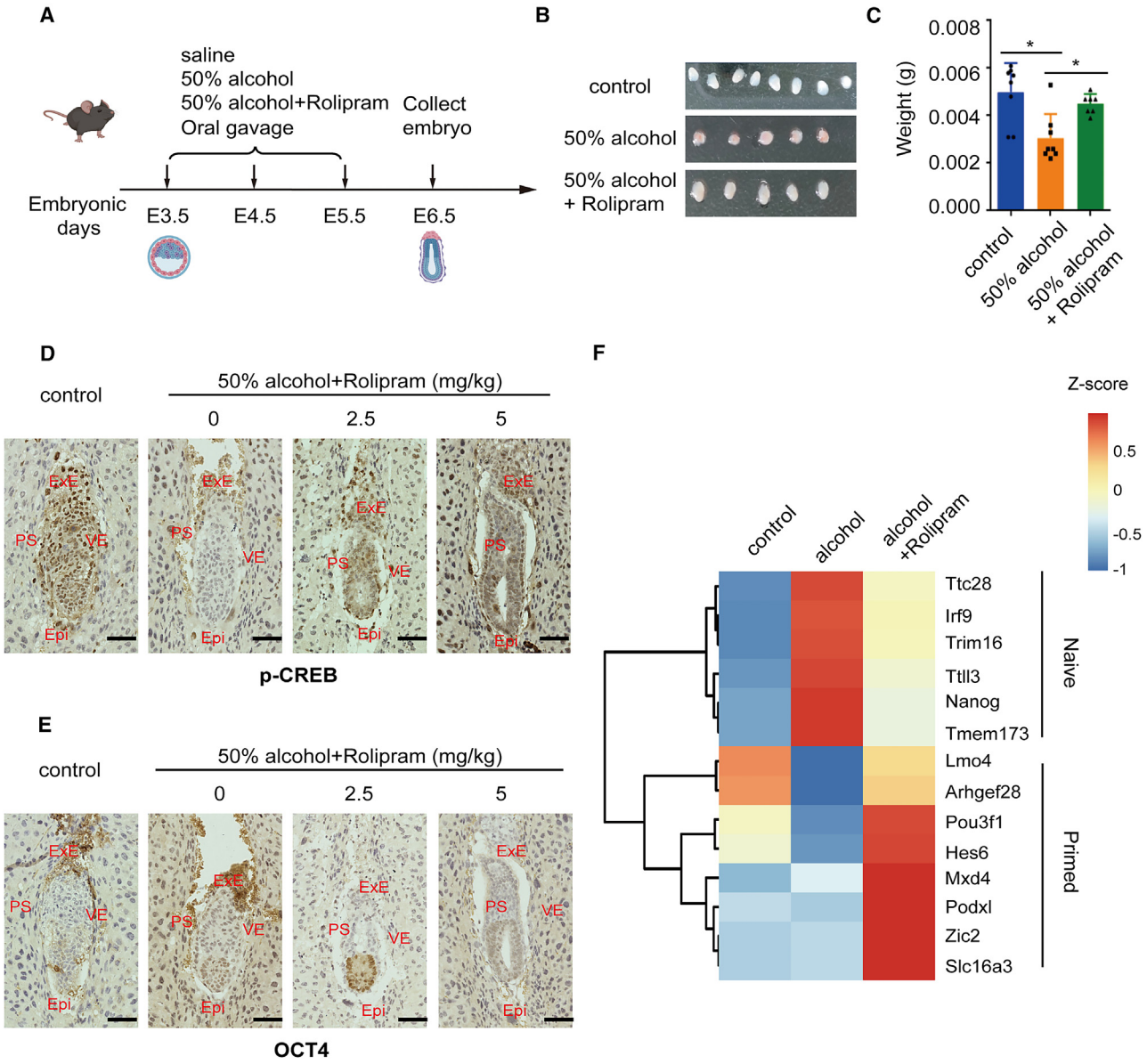

Figure 5. Rolipram alleviates post-implantation embryonic development delay caused by ethanol exposure

(A) Scheme of mouse models treated with rolipram following alcohol treatment at peri-implantation stage.

(B) Morphology of E6.5 embryos in control, alcohol-treated, and alcohol+rolipram-treated groups.

(C) Average weights of E6.5 embryos in the designated three groups. Data are represented as means ± SEM. Two-tailed unpaired t test. *$p < 0.05$; $n = 8$, 8, and 7, respectively, for the indicated three groups.

(D and E) Representative immunostaining of p-CREB (D) and OCT4 (E) in E6.5 embryos from the designated three groups. The staining was performed in three embryos from each group.

(F) Heatmap showing the relative expression of primed pluripotency genes in E6.5 epiblasts from the designated three groups. Gene expression levels are shown as relative *Z* scores across the samples.

See also Table S3.

Besides, our study establishes activated CREB as a pivotal link between ALDH treatment and KDM2B-dependent epigenomic alterations. Supporting this notion, a marked reduction in CREB expression and p-CREB levels has been observed in the amygdala following ethanol exposure.[48] More directly, ALDH has been found to diminish CREB activity in neuron-like cells,[47] potentially through a conserved response mechanism to cytotoxic stress. While CREB specifically regulates KDM2BLF expression, ALDH treatment results in the downregulation of both LF and SF expression levels (Figures 2G and 2H), which can be rescued by rolipram (Figures 4A and 4B). This suggests that additional transcription factors may function

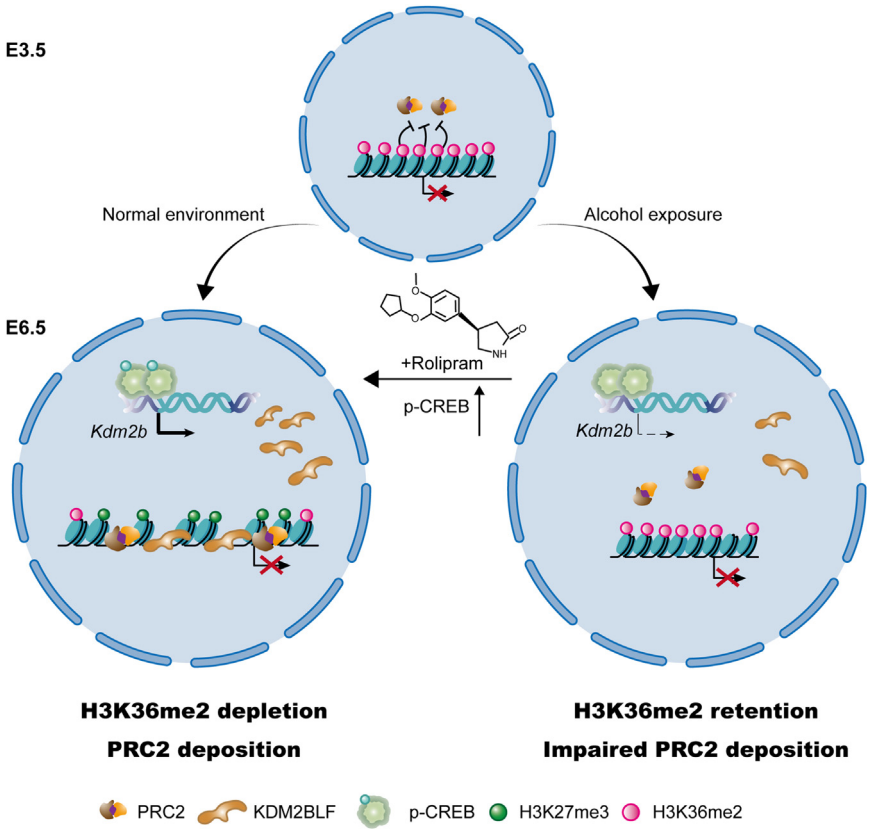

Figure 6. A model of the dysregulated CREB/KDM2BLF axis in ethanol-exposure-induced epigenetic rewiring and delayed post-implantation embryonic development

During the peri-implantation stage, embryos exposed to ethanol exhibit a failure to activate CREB, consequently impacting the transcriptional activation of its downstream target genes, including KDM2BLF. This disruption of the CREB/KDM2BLF axis impedes the establishment of PRC in post-implantation embryos, resulting in developmental delays. Rolipram, an anti-inflammatory drug, ameliorates these defects through enforced CREB activation and the subsequent associated epigenetic resetting.

downstream of ALDH treatment, and our data unveil that a KDM2B-independent regulatory mechanism may also contribute to the restoration of pluripotency transition by rolipram (Figures 4H and 4I). In turn, CREB activity is highly sensitive to a wide range of stimuli,[49] indicating the need to delineate an extensive transcriptional regulatory network along the CREB/KDM2B axis. This network is crucial for understanding development and pathogenesis, particularly in the context of ethanol exposure.

To date, no targeted interventions have been developed to address the developmental defects induced by ethanol exposure. This study underscores the significance of the dysregulated CREB/KDM2BLF axis as a pivotal mechanism in the epigenetic reprogramming elicited by ethanol. Promisingly, our research indicates that the restoration of CREB activity via PDE4 inhibitor treatment emerges as a potential preventive strategy, aimed at mitigating the adverse effects of ethanol on embryonic development during the critical peri-implantation phase.

Limitations of the study

While this study concentrates on the perturbed establishment of PRC functions at promoters, we acknowledge that other pathways may also contribute to the post-implantation developmental defects caused by ethanol. Regarding the rescue effects, our analysis was limited to the use of Rolipram on post-implantation development. The potential benefits of other PDE4 inhibitors warrant additional investigation. Furthermore, a more exhaustive examination of embryonic development, coupled with thorough evaluations of postnatal health and behavioral outcomes, is necessary to inform and guide future translational research endeavors.

RESOURCE AVAILABILITY

Lead contact

Further information and requests for resources and reagents should be directed to and will be fulfilled by the lead contact, Xudong Wu (wuxudong@tmu.edu.cn).

Materials availability

The plasmids and cell lines generated in this study are available upon request to the lead contact.

Data and code availability

- The RNA-seq and CUT&Tag raw datasets in this study have been deposited in GEO datasets under accession numbers GEO: GSE263480 and GSE263482.
- This paper does not report original code.
- Any additional information required to reanalyze the data reported in this paper is available from the lead contact upon request.

ACKNOWLEDGMENTS

We thank the Core Facility of Research Center of Basic Medical Sciences, High Performance Computing (HPC) Platform at Tianjin Medical University for technical support. We thank Dr. Fei Lan (Fudan Uni.) for a critical reading of the manuscript. This research was supported by grants from the National Natural

Science Foundation of China (32320103009 and 82473964), the National Key Research and Development Project of Stem Cell and Transformation Research (2019YFA0112100), the Key Research Project of Tianjin Education Commission (2020ZD13), the National Nonprofit Institute Research Grant of NRIFP (no. 2023GJZD01), and the National Youth Talent Support Program.

AUTHOR CONTRIBUTIONS

C.L. and X.W. conceived of and designed the study. H.L., M.G., Q.R., Y.Z., Q.L., D.H., Y.Y., Y.K., and X.L. performed cellular and molecular experiments, while H.L., Q.R., Y.Z., M.G., and Q.L. performed the mouse work. Q.L. and F.Z. did the bioinformatics analyses. H.L., L.C., and X.W. wrote the manuscript.

DECLARATION OF INTERESTS

X.W. is the inventor on the patent describing the PDE4 inhibitor in the prevention of embryonic development arrest caused by ethanol exposure.

STAR★METHODS

Detailed methods are provided in the online version of this paper and include the following:

- KEY RESOURCES TABLE
- EXPERIMENTAL MODEL AND STUDY PARTICIPANT DETAILS
  - Cell culture
- METHOD DETAILS
  - IHC and IF staining
  - AP staining
  - Real-time quantitative PCR
  - CUT&Tag
  - Sequencing data analysis
- QUANTIFICATION AND STATISTICAL ANALYSIS

SUPPLEMENTAL INFORMATION

Supplemental information can be found online at https://doi.org/10.1016/j.celrep.2024.115075.

Received: May 17, 2024
Revised: October 7, 2024
Accepted: November 25, 2024
Published: December 10, 2024

REFERENCES

1. Schuettengruber, B., Bourbon, H.M., Di Croce, L., and Cavalli, G. (2017). Genome Regulation by Polycomb and Trithorax: 70 Years and Counting. Cell *171*, 34–57. https://doi.org/10.1016/j.cell.2017.08.002.
2. Kim, J.J., and Kingston, R.E. (2022). Context-specific Polycomb mechanisms in development. Nat. Rev. Genet. *23*, 680–695. https://doi.org/10.1038/s41576-022-00499-0.
3. O'Carroll, D., Erhardt, S., Pagani, M., Barton, S.C., Surani, M.A., and Jenuwein, T. (2001). The polycomb-group gene Ezh2 is required for early mouse development. Mol. Cell Biol. *21*, 4330–4336. https://doi.org/10.1128/MCB.21.13.4330-4336.2001.
4. Pasini, D., Bracken, A.P., Jensen, M.R., Lazzerini Denchi, E., and Helin, K. (2004). Suz12 is essential for mouse development and for EZH2 histone methyltransferase activity. EMBO J. *23*, 4061–4071. https://doi.org/10.1038/sj.emboj.7600402.
5. Pasini, D., Bracken, A.P., Hansen, J.B., Capillo, M., and Helin, K. (2007). The polycomb group protein Suz12 is required for embryonic stem cell differentiation. Mol. Cell Biol. *27*, 3769–3779. https://doi.org/10.1128/MCB.01432-06.
6. Voncken, J.W., Roelen, B.A.J., Roefs, M., de Vries, S., Verhoeven, E., Marino, S., Deschamps, J., and van Lohuizen, M. (2003). Rnf2 (Ring1b) deficiency causes gastrulation arrest and cell cycle inhibition. Proc. Natl. Acad. Sci. USA *100*, 2468–2473. https://doi.org/10.1073/pnas.0434312100.
7. Zheng, H., Huang, B., Zhang, B., Xiang, Y., Du, Z., Xu, Q., Li, Y., Wang, Q., Ma, J., Peng, X., et al. (2016). Resetting Epigenetic Memory by Reprogramming of Histone Modifications in Mammals. Mol. Cell *63*, 1066–1079. https://doi.org/10.1016/j.molcel.2016.08.032.
8. Liu, X., Wang, C., Liu, W., Li, J., Li, C., Kou, X., Chen, J., Zhao, Y., Gao, H., Wang, H., et al. (2016). Distinct features of H3K4me3 and H3K27me3 chromatin domains in pre-implantation embryos. Nature *537*, 558–562. https://doi.org/10.1038/nature19362.
9. Marks, H., Kalkan, T., Menafra, R., Denissov, S., Jones, K., Hofemeister, H., Nichols, J., Kranz, A., Stewart, A.F., Smith, A., and Stunnenberg, H.G. (2012). The transcriptional and epigenomic foundations of ground state pluripotency. Cell *149*, 590–604. https://doi.org/10.1016/j.cell.2012.03.026.
10. Joshi, O., Wang, S.Y., Kuznetsova, T., Atlasi, Y., Peng, T., Fabre, P.J., Habibi, E., Shaik, J., Saeed, S., Handoko, L., et al. (2015). Dynamic Reorganization of Extremely Long-Range Promoter-Promoter Interactions between Two States of Pluripotency. Cell Stem Cell *17*, 748–757. https://doi.org/10.1016/j.stem.2015.11.010.
11. Fidalgo, M., Huang, X., Guallar, D., Sanchez-Priego, C., Valdes, V.J., Saunders, A., Ding, J., Wu, W.S., Clavel, C., and Wang, J. (2016). Zfp281 Coordinates Opposing Functions of Tet1 and Tet2 in Pluripotent States. Cell Stem Cell *19*, 355–369. https://doi.org/10.1016/j.stem.2016.05.025.
12. Weinberger, L., Ayyash, M., Novershtern, N., and Hanna, J.H. (2016). Dynamic stem cell states: naive to primed pluripotency in rodents and humans. Nat. Rev. Mol. Cell Biol. *17*, 155–169. https://doi.org/10.1038/nrm.2015.28.
13. Piunti, A., and Shilatifard, A. (2021). The roles of Polycomb repressive complexes in mammalian development and cancer. Nat. Rev. Mol. Cell Biol. *22*, 326–345. https://doi.org/10.1038/s41580-021-00341-1.
14. Gong, M., Yuan, Y., Dai, Z., Lv, X., Su, J., Huo, D., Niu, L., Chen, X., and Wu, X. (2024). PRC2 primes bivalent genes for transcription induction independent of histone methyltransferase activity. Sci. China Life Sci. *67*, 2033–2035. https://doi.org/10.1007/s11427-024-2573-2.
15. Huo, D., Yu, Z., Li, R., Gong, M., Sidoli, S., Lu, X., Hou, Y., Dai, Z., Kong, Y., Liu, G., et al. (2022). CpG island reconfiguration for the establishment and synchronization of polycomb functions upon exit from naive pluripotency. Mol. Cell *82*, 1169–1185.e7. https://doi.org/10.1016/j.molcel.2022.01.027.
16. Wu, X., Johansen, J.V., and Helin, K. (2013). Fbxl10/Kdm2b recruits polycomb repressive complex 1 to CpG islands and regulates H2A ubiquitylation. Mol. Cell *49*, 1134–1146. https://doi.org/10.1016/j.molcel.2013.01.016.
17. He, J., Kallin, E.M., Tsukada, Y.I., and Zhang, Y. (2008). The H3K36 demethylase Jhdm1b/Kdm2b regulates cell proliferation and senescence through p15(Ink4b). Nat. Struct. Mol. Biol. *15*, 1169–1175. https://doi.org/10.1038/nsmb.1499.
18. Fukuda, T., Tokunaga, A., Sakamoto, R., and Yoshida, N. (2011). Fbxl10/Kdm2b deficiency accelerates neural progenitor cell death and leads to exencephaly. Mol. Cell. Neurosci. *46*, 614–624. https://doi.org/10.1016/j.mcn.2011.01.001.
19. Jégou, S., El Ghazi, F., de Lendeu, P.K., Marret, S., Laudenbach, V., Uguen, A., Marcorelles, P., Roy, V., Laquerriere, A., and Gonzalez, B.J. (2012). Prenatal alcohol exposure affects vasculature development in the neonatal brain. Ann. Neurol. *72*, 952–960. https://doi.org/10.1002/ana.23699.
20. Zhong, L., Zhu, J., Lv, T., Chen, G., Sun, H., Yang, X., Huang, X., and Tian, J. (2010). Ethanol and its metabolites induce histone lysine 9 acetylation and an alteration of the expression of heart development-related genes in cardiac progenitor cells. Cardiovasc. Toxicol. *10*, 268–274. https://doi.org/10.1007/s12012-010-9081-z.

21. Brien, J.F., Loomis, C.W., Tranmer, J., and McGrath, M. (1983). Disposition of ethanol in human maternal venous blood and amniotic fluid. Am. J. Obstet. Gynecol. *146*, 181–186. https://doi.org/10.1016/0002-9378(83)91050-5.

22. Ikonomidou, C., Bittigau, P., Ishimaru, M.J., Wozniak, D.F., Koch, C., Genz, K., Price, M.T., Stefovska, V., Hörster, F., Tenkova, T., et al. (2000). Ethanol-induced apoptotic neurodegeneration and fetal alcohol syndrome. Science *287*, 1056–1060. https://doi.org/10.1126/science.287.5455.1056.

23. Legault, L.M., Bertrand-Lehouillier, V., and McGraw, S. (2018). Pre-implantation alcohol exposure and developmental programming of FASD: an epigenetic perspective. Biochem. Cell. Biol. *96*, 117–130. https://doi.org/10.1139/bcb-2017-0141.

24. Veazey, K.J., Carnahan, M.N., Muller, D., Miranda, R.C., and Golding, M.C. (2013). Alcohol-induced epigenetic alterations to developmentally crucial genes regulating neural stemness and differentiation. Alcohol Clin. Exp. Res. *37*, 1111–1122. https://doi.org/10.1111/acer.12080.

25. Kaminen-Ahola, N., Ahola, A., Maga, M., Mallitt, K.A., Fahey, P., Cox, T.C., Whitelaw, E., and Chong, S. (2010). Maternal Ethanol Consumption Alters the Epigenotype and the Phenotype of Offspring in a Mouse Model. PLoS Genet. *6*, e1000811. https://doi.org/10.1371/journal.pgen.1000811.

26. Garro, A.J., McBeth, D.L., Lima, V., and Lieber, C.S. (1991). Ethanol consumption inhibits fetal DNA methylation in mice: implications for the fetal alcohol syndrome. Alcohol Clin. Exp. Res. *15*, 395–398. https://doi.org/10.1111/j.1530-0277.1991.tb00536.x.

27. Pan, B., Zhu, J., Lv, T., Sun, H., Huang, X., and Tian, J. (2014). Alcohol consumption during gestation causes histone3 lysine9 hyperacetylation and an alternation of expression of heart development-related genes in mice. Alcohol Clin. Exp. Res. *38*, 2396–2402. https://doi.org/10.1111/acer.12518.

28. Dumas, R.M., and Rabe, A. (1994). Augmented memory loss in aging mice after one embryonic exposure to alcohol. Neurotoxicol. Teratol. *16*, 605–612. https://doi.org/10.1016/0892-0362(94)90038-8.

29. Neagu, A., van Genderen, E., Escudero, I., Verwegen, L., Kurek, D., Lehmann, J., Stel, J., Dirks, R.A.M., van Mierlo, G., Maas, A., et al. (2020). In vitro capture and characterization of embryonic rosette-stage pluripotency between naive and primed states. Nat. Cell Biol. *22*, 534–545. https://doi.org/10.1038/s41556-020-0508-x.

30. Kottakis, F., Polytarchou, C., Foltopoulou, P., Sanidas, I., Kampranis, S.C., and Tsichlis, P.N. (2011). FGF-2 Regulates Cell Proliferation, Migration, and Angiogenesis through an NDY1/KDM2B-miR-101-EZH2 Pathway. Mol. Cell *43*, 285–298. https://doi.org/10.1016/j.molcel.2011.06.020.

31. Naqvi, S., Martin, K.J., and Arthur, J.S.C. (2014). CREB phosphorylation at Ser133 regulates transcription via distinct mechanisms downstream of cAMP and MAPK signalling. Biochem. J. *458*, 469–479. https://doi.org/10.1042/BJ20131115.

32. Fernandes, N.D., Sun, Y., and Price, B.D. (2007). Activation of the kinase activity of ATM by retinoic acid is required for CREB-dependent differentiation of neuroblastoma cells. J. Biol. Chem. *282*, 16577–16584. https://doi.org/10.1074/jbc.M609628200.

33. Bleckmann, S.C., Blendy, J.A., Rudolph, D., Monaghan, A.P., Schmid, W., and Schütz, G. (2002). Activating transcription factor 1 and CREB are important for cell survival during early mouse development. Mol. Cell Biol. *22*, 1919–1925. https://doi.org/10.1128/MCB.22.6.1919-1925.2002.

34. Li, R., Xia, X., Wang, X., Sun, X., Dai, Z., Huo, D., Zheng, H., Xiong, H., He, A., and Wu, X. (2020). Generation and validation of versatile inducible CRISPRi embryonic stem cell and mouse model. PLoS Biol. *18*, e3000749. https://doi.org/10.1371/journal.pbio.3000749.

35. Iacovino, M., Bosnakovski, D., Fey, H., Rux, D., Bajwa, G., Mahen, E., Mitanoska, A., Xu, Z., and Kyba, M. (2011). Inducible cassette exchange: a rapid and efficient system enabling conditional gene expression in embryonic stem and primary cells. Stem Cell. *29*, 1580–1588. https://doi.org/10.1002/stem.715.

36. Tibbo, A.J., Tejeda, G.S., and Baillie, G.S. (2019). Understanding PDE4's function in Alzheimer's disease; a target for novel therapeutic approaches. Biochem. Soc. Trans. *47*, 1557–1565. https://doi.org/10.1042/BST20190763.

37. Martinez, A., and Gil, C. (2014). cAMP-specific phosphodiesterase inhibitors: promising drugs for inflammatory and neurological diseases. Expert Opin. Ther. Pat. *24*, 1311–1321. https://doi.org/10.1517/13543776.2014.968127.

38. Fujioka, T., Fujioka, A., and Duman, R.S. (2004). Activation of cAMP signaling facilitates the morphological maturation of newborn neurons in adult hippocampus. J. Neurosci. *24*, 319–328. https://doi.org/10.1523/JNEUROSCI.1065.03.2004.

39. Tian, F.Y., and Marsit, C.J. (2018). Environmentally Induced Epigenetic Plasticity in Development: Epigenetic Toxicity and Epigenetic Adaptation. Curr. Epidemiol. Rep. *5*, 450–460. https://doi.org/10.1007/s40471-018-0175-7.

40. Popova, S., Charness, M.E., Burd, L., Crawford, A., Hoyme, H.E., Mukherjee, R.A.S., Riley, E.P., and Elliott, E.J. (2023). Fetal alcohol spectrum disorders. Nat. Rev. Dis. Prim. *9*, 11. https://doi.org/10.1038/s41572-023-00420-x.

41. Jarmasz, J.S., Stirton, H., Basalah, D., Davie, J.R., Clarren, S.K., Astley, S.J., and Del Bigio, M.R. (2019). Global DNA Methylation and Histone Posttranslational Modifications in Human and Nonhuman Primate Brain in Association with Prenatal Alcohol Exposure. Alcohol Clin. Exp. Res. *43*, 1145–1162. https://doi.org/10.1111/acer.14052.

42. Kaminen-Ahola, N. (2020). Fetal alcohol spectrum disorders: Genetic and epigenetic mechanisms. Prenat. Diagn. *40*, 1185–1192. https://doi.org/10.1002/pd.5731.

43. Mews, P., Egervari, G., Nativio, R., Sidoli, S., Donahue, G., Lombroso, S.I., Alexander, D.C., Riesche, S.L., Heller, E.A., Nestler, E.J., et al. (2019). Alcohol metabolism contributes to brain histone acetylation. Nature *574*, 717–721. https://doi.org/10.1038/s41586-019-1700-7.

44. Mandal, C., Halder, D., Jung, K.H., and Chai, Y.G. (2017). In utero alcohol exposure and the alteration of histone marks in the developing fetus: an epigenetic phenomenon of maternal drinking. Int. J. Biol. Sci. *13*, 1100–1108. https://doi.org/10.7150/ijbs.21047.

45. Ungerer, M., Knezovich, J., and Ramsay, M. (2013). In utero alcohol exposure, epigenetic changes, and their consequences. Alcohol Res. *35*, 37–46.

46. Basavarajappa, B.S. (2023). Epigenetics in fetal alcohol spectrum disorder. Prog. Mol. Biol. Transl. Sci. *197*, 211–239. https://doi.org/10.1016/bs.pmbts.2023.01.004.

47. Yan, T., Zhao, Y., Zhang, X., and Lin, X. (2016). Astaxanthin Inhibits Acetaldehyde-Induced Cytotoxicity in SH-SY5Y Cells by Modulating Akt/CREB and p38MAPK/ERK Signaling Pathways. Mar. Drugs *14*, 56. https://doi.org/10.3390/md14030056.

48. Zhang, H., Kyzar, E.J., Bohnsack, J.P., Kokare, D.M., Teppen, T., and Pandey, S.C. (2018). Adolescent alcohol exposure epigenetically regulates CREB signaling in the adult amygdala. Sci. Rep. *8*, 10376. https://doi.org/10.1038/s41598-018-28415-9.

49. Shaywitz, A.J., and Greenberg, M.E. (1999). CREB: a stimulus-induced transcription factor activated by a diverse array of extracellular signals. Annu. Rev. Biochem. *68*, 821–861. https://doi.org/10.1146/annurev.biochem.68.1.821.

50. McQuin, C., Goodman, A., Chernyshev, V., Kamentsky, L., Cimini, B.A., Karhohs, K.W., Doan, M., Ding, L., Rafelski, S.M., Thirstrup, D., et al. (2018). CellProfiler 3.0: Next-generation image processing for biology. PLoS Biol. *16*, e2005970. https://doi.org/10.1371/journal.pbio.2005970.

51. Schneider, C.A., Rasband, W.S., and Eliceiri, K.W. (2012). NIH Image to ImageJ: 25 years of image analysis. Nat. Methods *9*, 671–675. https://doi.org/10.1038/nmeth.2089.

52. Zhang, Y., Liu, T., Meyer, C.A., Eeckhoute, J., Johnson, D.S., Bernstein, B.E., Nusbaum, C., Myers, R.M., Brown, M., Li, W., and Liu, X.S. (2008).

Model-based analysis of ChIP-Seq (MACS). Genome Biol. *9*, R137. https://doi.org/10.1186/gb-2008-9-9-r137.

53. Trapnell, C., Pachter, L., and Salzberg, S.L. (2009). TopHat: discovering splice junctions with RNA-Seq. Bioinformatics *25*, 1105–1111. https://doi.org/10.1093/bioinformatics/btp120.
54. Park, S.H., Seo, W., Xu, M.J., Mackowiak, B., Lin, Y., He, Y., Fu, Y., Hwang, S., Kim, S.J., Guan, Y., et al. (2023). Ethanol and its Nonoxidative Metabolites Promote Acute Liver Injury by Inducing ER Stress, Adipocyte Death, and Lipolysis. Cell. Mol. Gastroenterol. Hepatol. *15*, 281–306. https://doi.org/10.1016/j.jcmgh.2022.10.002.
55. Wu, X., Bekker-Jensen, I.H., Christensen, J., Rasmussen, K.D., Sidoli, S., Qi, Y., Kong, Y., Wang, X., Cui, Y., Xiao, Z., et al. (2015). Tumor suppressor ASXL1 is essential for the activation of INK4B expression in response to oncogene activity and anti-proliferative signals. Cell Res. *25*, 1205–1218. https://doi.org/10.1038/cr.2015.121.
56. Dong, F., Li, Q., Yang, C., Huo, D., Wang, X., Ai, C., Kong, Y., Sun, X., Wang, W., Zhou, Y., et al. (2018). PRMT2 links histone H3R8 asymmetric dimethylation to oncogenic activation and tumorigenesis of glioblastoma. Nat. Commun. *9*, 4552. https://doi.org/10.1038/s41467-018-06968-7.
57. Dai, Z., Li, R., Hou, Y., Li, Q., Zhao, K., Li, T., Li, M.J., and Wu, X. (2021). Inducible CRISPRa screen identifies putative enhancers. J. Genet. Genom. *48*, 917–927. https://doi.org/10.1016/j.jgg.2021.06.012.
58. Cao, L., Han, R., Zhao, Y., Qin, X., Li, Q., Xiong, H., Kong, Y., Liu, Z., Li, Z., Dong, F., et al. (2024). A LATS2 and ALKBH5 positive feedback loop supports their oncogenic roles. Cell Rep. *43*, 114032. https://doi.org/10.1016/j.celrep.2024.114032.
59. Pertea, M., Pertea, G.M., Antonescu, C.M., Chang, T.C., Mendell, J.T., and Salzberg, S.L. (2015). StringTie enables improved reconstruction of a transcriptome from RNA-seq reads. Nat. Biotechnol. *33*, 290–295. https://doi.org/10.1038/nbt.3122.
60. Langmead, B., and Salzberg, S.L. (2012). Fast gapped-read alignment with Bowtie 2. Nat. Methods *9*, 357–359. https://doi.org/10.1038/nmeth.1923.
61. Ramírez, F., Ryan, D.P., Gruning, B., Bhardwaj, V., Kilpert, F., Richter, A.S., Heyne, S., Dundar, F., and Manke, T. (2016). deepTools2: a next generation web server for deep-sequencing data analysis. Nucleic Acids Res. *44*, W160–W165. https://doi.org/10.1093/nar/gkw257.

STAR★METHODS

KEY RESOURCES TABLE

REAGENT or RESOURCE	SOURCE	IDENTIFIER
Antibodies		
Rabbit polyclonal anti-Nanog	Bethyl	Cat#A300-397A;RRID:AB_386108
Rabbit polyclonal anti-GAPDH	Abclonal	Cat# AC002; RRID: AB_2736879
Rabbit polyclonal anti-KDM2B	home-made	N/A
Rabbit monoclonal anti-H3K27me3	Cell Signaling Technology	Cat#9733; RRID:AB_2616029
Rabbit monoclonal anti-H2AK119ub1	Cell Signaling Technology	Cat#8240; RRID:AB_10891618
Rabbit monoclonal anti-H3K36me2	Cell Signaling Technology	Cat#2901; RRID:AB_1030983
Rabbit monoclonal anti-*p*-CREB	Cell Signaling Technology	Cat#9198; RRID:AB_2561044
Rabbit monoclonal anti-CREB	Cell Signaling Technology	Cat#9197; RRID:AB_331277
Mouse monoclonal anti-FLAG	Abclonal	Cat# AE005; RRID: AB_3095798
Mouse monoclonal anti-Pan acetyl lysine	Abclonal	Cat#A1525; RRID:AB_2762147
Rabbit monoclonal anti-β-ACTIN	Abclonal	Cat# AC026; RRID: AB_2768234
Bacterial and virus strains		
DH5α	home-made	N/A
TransDB3.1 Chemically Competent Cell	TransGen Biotech	CD531-01
Chemicals, peptides, and recombinant proteins		
GSK inhibitor	Selleck	S2924
MEK inhibitor	Selleck	S1036
recombinant mouse lif	Sinobiological	50756-MNAH-20
mouse Activin A protein (His tag)	Sinobiological	50659-M08H-20
recombinant mouse FGF2 Protein	Sinobiological	50659-M08H-20
Puromycin	Sigma-Aldrich	P8833-25MG
Doxycycline hyclate	Sigma-Aldrich	D9891-10G
N2	Gibco	D9891-10G
B27	Gibco	17504044
compound 3i (666-15)	Selleck	S8846
Rolipram (Synonyms: (R,S)-Rolipram; SB 95952; ZK 62711)	MedChemExpress	CAS No. : 61413-54-5 HY16900
alcohol	J&K Scientific	CAS:64-17-5
acetaldehyde	J&K Scientific	CAS:75-07-0
acetic acid	J&K Scientific	CAS:64-19-7
Critical commercial assays		
Gateway LR Clonase II Enzyme mix	Thermo Fisher	Cat#11791020
Hyperactive pA-Tn5 Transposase for CUT&Tag	Vazyme	S603
trueprep DNA library prep kit V2 for illuminated	Vazyme	TD501; TD503
VAHTS Universal V8 RNA-seq Library Prep Kit for Illumina	Vazyme	NR605-01
VAHTS RNA Adapters Set 1 - Set 2 for Illumina	Vazyme	N803/N804
VAHTS mRNA Capture Beads	Vazyme	N403
Deposited data		
Raw and analyzed data	This paper	GEO: GSE263482, GSE263480
Experimental models: Cell lines		
WT (E14) mESC	Helin lab	N/A
A2Loxcre mESC	Iacovino et al.[35]	N/A

(*Continued on next page*)

Continued		
REAGENT or RESOURCE	SOURCE	IDENTIFIER
293FT cells	Helin lab	N/A
KDM2BLF KO mESC	This paper	N/A
Experimental models: Organisms/strains		
Mouse: C57BL/6J	Charles River	C57BL/6J
Oligonucleotides		
see Table S4	This paper	N/A
Software and algorithms		
CellProfiler	McQuin et al.[50]	https://cellprofiler.org
ImageJ	Schneider et al.[51]	https://imagej.nih.gov/ij/
Other		
MACS2 (v2.1.1.20160309)	Zhang et al., 2008[52]	https://pypi.org/project/MACS2/
TopHat (v2.1.1)	Trapnell et al., 2009[53]	https://ccb.jhu.edu/software/tophat/index.shtml

EXPERIMENTAL MODEL AND STUDY PARTICIPANT DETAILS

Cell culture

Cell lines, cell culture and treatment

293FT cells were cultured in DMEM (GIBCO) and 10% FBS (Lonsera). Mouse embryonic stem cells (E14) were cultured in 0.2% gelatin-coated Petri dishes in either 2iL, SL or FA culture medium as described.[15] To determine the ALDH concentration for the *in vitro* assay, we calculated the serum ALDH concentration in mice. According to previous studies, within 10 h after ethanol gavage, the ALDH concentration in serum is 1–2 μg/mL.[54] Given that the density of 40% acetaldehyde is 0.788 g/mL, we treated mESCs with ALDH in the culture medium at 10 or 20 mM, which is 0.985 μg/mL or 1.97 μg/mL and comparable to the serum ALDH concentration. The cells were detected by mycoplasma without mycoplasma contamination.

Generation of CREB-depleted mESCs

Specific oligos against CREB (listed in Table S4) were annealed and inserted into the pLKO-TRC cloning vector. For the production of viral particles, the pLKO-shCREB lentiviral vectors were co-transfected with PAX8 and VSVG into 293T cells. The virus-containing medium was then collected 48 h after transfection, and mESCs were spin infected as described.[55] Polybrene was added to the viral medium at a concentration of 8 μg/mL and transduced cells were selected by puromycin (2 μg/mL) for 2 days.

Construction of A2LoxCre-CREBS133D cells lines

The full-length PCR fragment of CREB was cloned into pCR8 entry vector (Thermofisher) and the S133D mutation was generated accordingly.[56] The primer sequences are listed in Table S4. Then the mutant was cloned into the p2Lox-FLAG vector[35] through recombination. Subsequently, the A2LoxCre mESCs were transfected with the p2Lox-FLAG-CREBS133D plasmids after 16 h of DOX treatment, followed by G418 selection (50 mg/mL) for 7 days. Single colonies were isolated after about 7 days, expanded, and selected as described.[57] And the DOX inducible expression of FLAG-CREBS133D protein was tested by WB assay.

Ethanol exposure models for mouse peri-implantation embryos and Rolipram administration

C57BL/6 mice (8 weeks old) were purchased from Beijing Vital River Laboratory Animal Technology Co., Ltd. The mice were treated in accordance with the NIH Guide for the Care and Use of Laboratory Animals. All the protocols had the approval of the Institutional Committee on Animal Care and Use of the National Research Institute for Family Planning. After being maintained in house for another 3 weeks, mice were caged in a 2:1 ratio of females to males. Embryonic day 0.5 (E0.5) was defined as the morning when the vaginal plug was observed in female mice. Alcohol concentration was divided into three dosage groups, 0%, 25%, and 50%. Edible alcohol was diluted to the desired concentration with saline. Gavage was performed according to a gavage volume of 10 μL per gram of mouse body weights,[27,28] starting on day E3.5 and continuing until E5.5. On day E6.5, the female mice were euthanized by cervical dislocation. The embryos were isolated and the mass of each embryo was weighed, followed by either IHC, RNA-seq or CUT&Tag analysis. To rescue the development of ethanol-exposure embryos, Rolipram (MedChemExpress, HY-16900) was prepared according to the manufacturer's protocol. For the pregnant mice treated with 50% alcohol, 2.5 mg/kg and 5 mg/kg Rolipram was administrated simultaneously through intraperitoneal injection for three consecutive days.

METHOD DETAILS

IHC and IF staining

E6.5 embryos were collected for tissue embedding and sectioning. Then the tissue slides from were de-paraffinized, rehydrated through an alcohol series followed by antigen retrieval with sodium citrate buffer. After the inactivation of endogenous catalase and permeabilization with 0.5% Triton X-100 for 5min, the sections were blocked with goat serum containing with 0.1% Triton

X-100 in PBS for 1 h at room temperature and incubated overnight with primary antibodies 4°C overnight. IHC staining was performed with HRP conjugates using DAB detection. When the brown particles appeared on the tissue, the reaction was terminated.[58]

For the IF analysis of cultured cells, ESCs were fixed with 4% formaldehyde (Fisher) for 15 min. After being washed twice with PBS, the cells were incubated with 0.8% BSA (A80209, solarbio) with 0.1% Triton X-100 in PBS for 10 min. The primary antibody NANOG (A300-397A, Bethyl) was diluted 1:100 with PBS and then incubated with cells at 4°C overnight. After being washed five times with PBS, the secondary antibody was incubated at room temperature for 1 h. The slices were blocked by DAPI staining for 10 min. Images were captured by confocal fluorescence microscopy and analyzed with CellProfiler image analysis software.

AP staining

In order to compare the pluripotency of ES cells under various culture conditions, the cells were fixed with 4% paraformaldehyde for 20 min. After the cells were stained with an AP staining kit (C3206, Beyotime), images were acquired.

Real-time quantitative PCR

To quantify the gene expression at mRNA levels, total RNA was extracted with TRIzol (15596026, Thermo) and reverse transcribed with a revertAid first strand cDNA synthesis kit (K1622, Thermo). Then quantitative PCR analyses of cDNA were performed with ChamQ Universal SYBR qPCR Master Mix (Q711, Vazyme) on Roche LightCycler 480 system. The primer sequences were listed in Table S4.

CUT&Tag

Epiblasts were isolated and washed twice in 1 mL washing buffer (20 mM HEPES PH 7.5, 150 mM NaCl, 0.5 mM Spermidine, 1×PIC, and then resuspended in 300 μL washing buffer. The following processes were conducted as described[15] at room temperature unless otherwise stated. Concanavalin A coated beads were activated by washing twice in binding buffer (20 mM HEPES pH 7.5, 10 mM KCl, 1mM $MnCl_2$, 1mM $CaCl_2$). Then 10 μL activated beads were incubated with the resuspended cells for 30 min. The supernatant was removed and beads were resuspended in 50 μL antibody buffer (20 mM HEPES pH 7.5,150 mM NaCl, 0.5 mM Spermidine, 0.0125% Digitonin, 2 mM EDTA, 0.1% BSA, 1×PIC). Then 0.5 μL primary antibody was added and incubated for 2 h. After the supernatant was gently removed by placing the tubes on magnet, the beads were resuspended in 100 μL Dig washing buffer (20 mM HEPES pH 7.5, 150 mM NaCl, 0.5 mM Spermidine, 0.0125% Digitonin, 1×PIC) which contains 1 μL Guinea Pig anti-Rabbit IgG antibody and incubated for 1 h. After being washed three times in 800 μL Dig wash buffer, the beads were resuspended in 100 μL Dig 300 washing buffer (20 mM HEPES pH 7.5, 300 mM NaCl, 0.5 mM Spermidine, 0.0125% Digitonin, 1×PIC), and 0.04 μM pA-Tn5 adapter complex (Vazyme S603) was added and incubated for 1 h. Beads were washed three times in 800 μL Dig 300 washing buffer and resuspended in 300 μL tagmentation buffer (20 mM HEPES pH 7.5, 300 mM NaCl, 0.5 mM Spermidine, 0.0125% Digitonin, 10 mM $MgCl_2$, 1×PIC) and incubated for 1 h at 37°C. Subsequently 10 μL of 0.5 M EDTA, 3 μL of 10% SDS and 1 μL of 20 mg/mL Proteinase K were added and incubated at 55°C for 1 h to stop tagmentation before DNA extraction by PCI. The purified DNA was amplified with i5 and i7 primer, KAPA 2x PCR mix (KM2602), under the cycling program with heated lid, 72°C, 5 min; 98°C, 30 s; 17 cycles for 98°C, 10s; 60°C, 30 s; 72°C, 30 s; and 72°C for 5 min, hold at 4°C. After the program was completed, 0.5 volume (25 μL) Ampure XP beads were added to remove fragments above 1 kb and another 0.5 volume (25 μL) were added to enrich the 200-1,000bp fragments for library preparation. The successfully constructed libraries were sequenced with PE150 on NovaSeq platform.

Sequencing data analysis

RNA-seq reads were aligned to mouse genome build mm10 using Hisat2 V2.2.1. Expression levels for all RefSeq transcripts were quantified to fragment per kilobase million (FPKM) using StringTie v2.1.1.[59]

CUT&Tag reads were first processed using TrimGalore (v0.4.4_dev) to trim adaptor and low-quality reads. Trimmed reads were then aligned to the mouse genome build mm10 using bowtie2 (v2.4.2)[60] with parameters "–local –very-sensitive –no-mixed –no-discordant –phred33 -I 10 -X 700". Low mapping quality reads (mapping quality <30) and duplicates were discarded. Then biological replicates passed quality control were pooled together. Heatmap, profile and Signal tracks for each sample were generated using deeptools V3.5.1.[61] Peak calling was performed by MACS2.[52]

QUANTIFICATION AND STATISTICAL ANALYSIS

No statistical methods were used to predetermine sample sizes, but our sample sizes are similar to those reported in previous publications. The experiments were not randomized, and investigators were not blinded to allocation during experiments. Unpaired Student's *t*-tests are presented as mean ± SEM during comparison between unpaired two-groups. Sample sizes and experimental replicates and specific statistical tests used are described in the Figure Legends. Data were plotted using GraphPad Prism 9 software as mean values. Significant difference is indicated by a *p* value less than 0.05 (*$p < 0.05$, **$p < 0.01$, ***$p < 0.001$, ****$p < 0.0001$).

Cell Reports, Volume *43*

Supplemental information

Enforced activation of the CREB/KDM2B axis prevents alcohol-induced embryonic developmental delay

Hang Liu, Qiyu Ren, Meihan Gong, Feifei Zuo, Qian Li, Dawei Huo, Ye Yuan, Yutong Zhang, Yu Kong, Xiaozhi Liu, Cailing Lu, and Xudong Wu

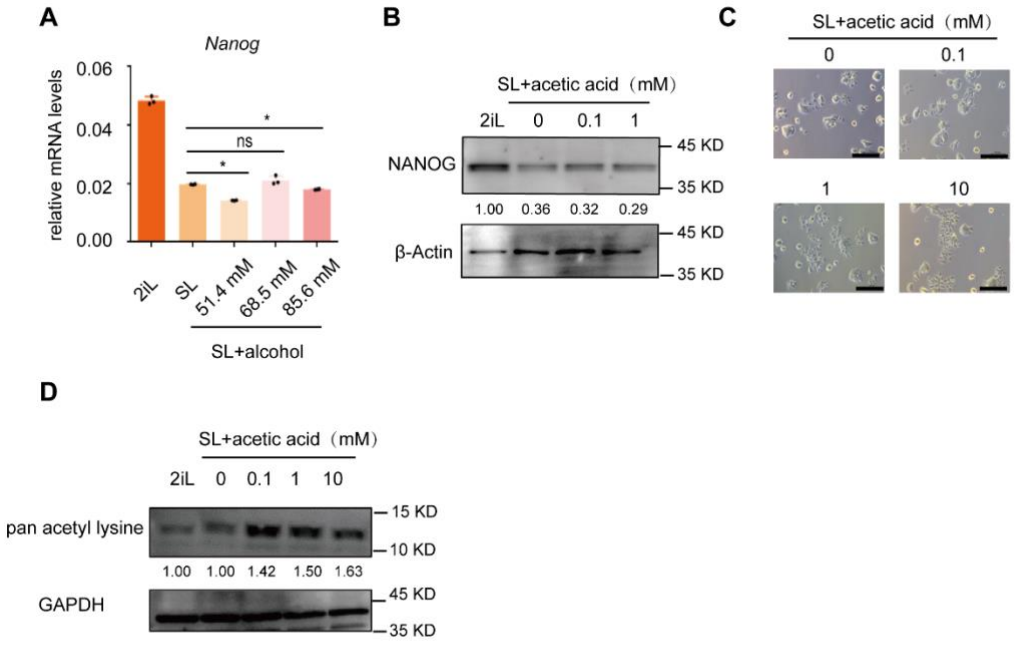

Figure S1. Ethanol or acetate does not delay the exit from naive pluripotency. Related to Figure 1.

(**A**) RT-qPCR analysis of NANOG expression levels in mESCs cultured under 2iL condition or SL conditions treated with varying concentrations of ethanol. Data are represented as means ± SEM. Statistical tests were performed using two-tailed unpaired *t* test with Welch's correction. **P* < 0.05. n.s. nonsignificant. (**B**) WB analysis comparing NANOG expression levels in mESCs cultured under 2iL condition or SL conditions treated with different concentrations of acetic acid. (**C**) Morphology of mESCs subgrouped as (**B**). Scale bars, 100 μm. (**D**) WB analysis comparing pan acetyl lysine levels in mESCs subgrouped as (**B**). β-ACTIN and GAPDH serves as loading controls respectively in (**B**) and (**D**).

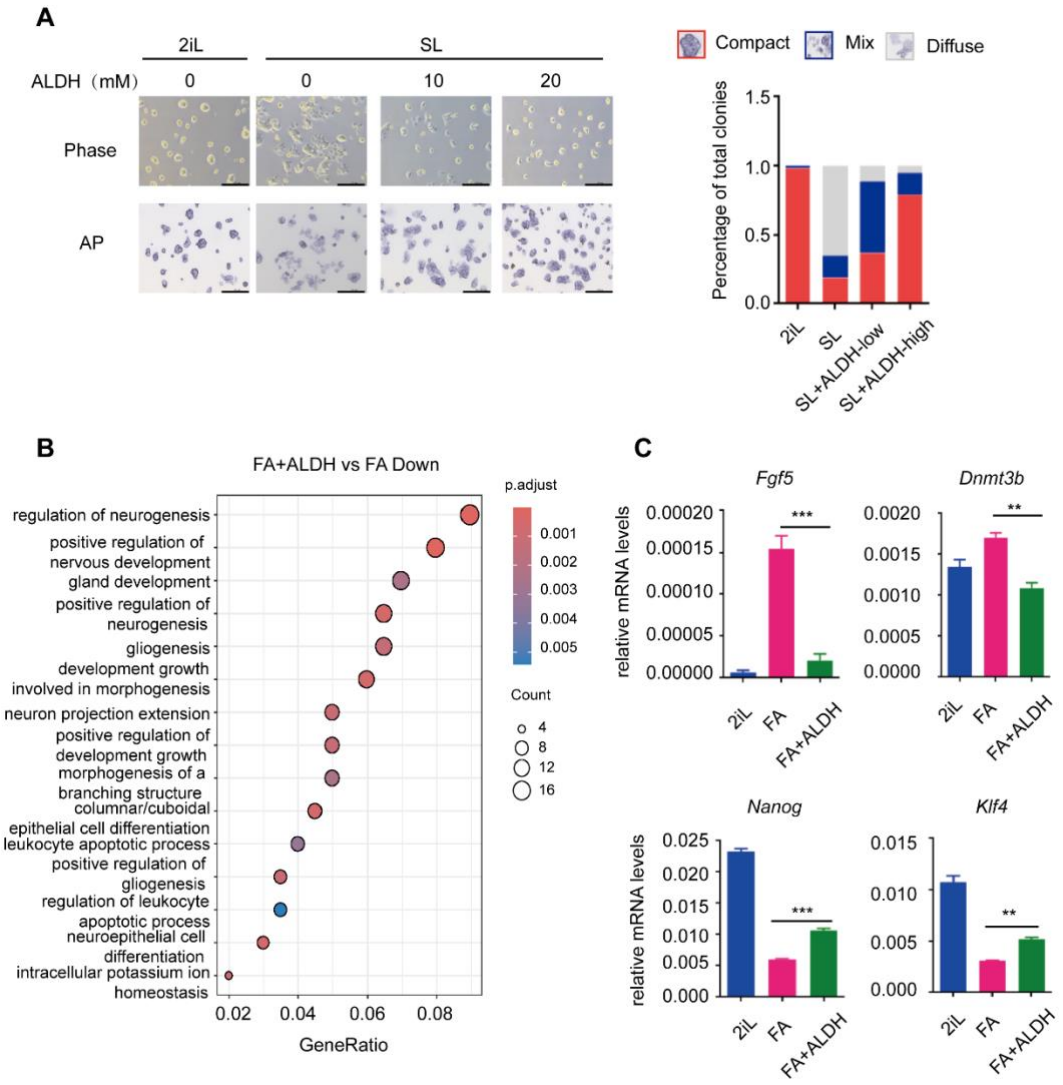

Figure S2. ALDH treatment causes delayed exit from naive pluripotency. Related to Figure 1.

(**A**) Morphology and AP staining of mESCs cultured under 2iL condition or SL conditions treated with different concentrations of ALDH (left). The boxplots showing the quantification of the morphology (Compact, Mix, Diffuse) of the cells in different conditions (right). Gray represents diffuse, blue represents mix and red represents compact. (**B**) Highly enriched GO biological processes of downregulated genes by ALDH in FA-mESCs, performed using R package clusterProfiler. (**C**) RT-qPCR analysis of representative primed and naive pluripotency genes in 2iL, FA, FA+ALDH- mESCs. Data are represented as means ± SEM. Statistical tests were performed using two-tailed unpaired *t* test with Welch's correction. ** P <0.01; *** P <0.001.

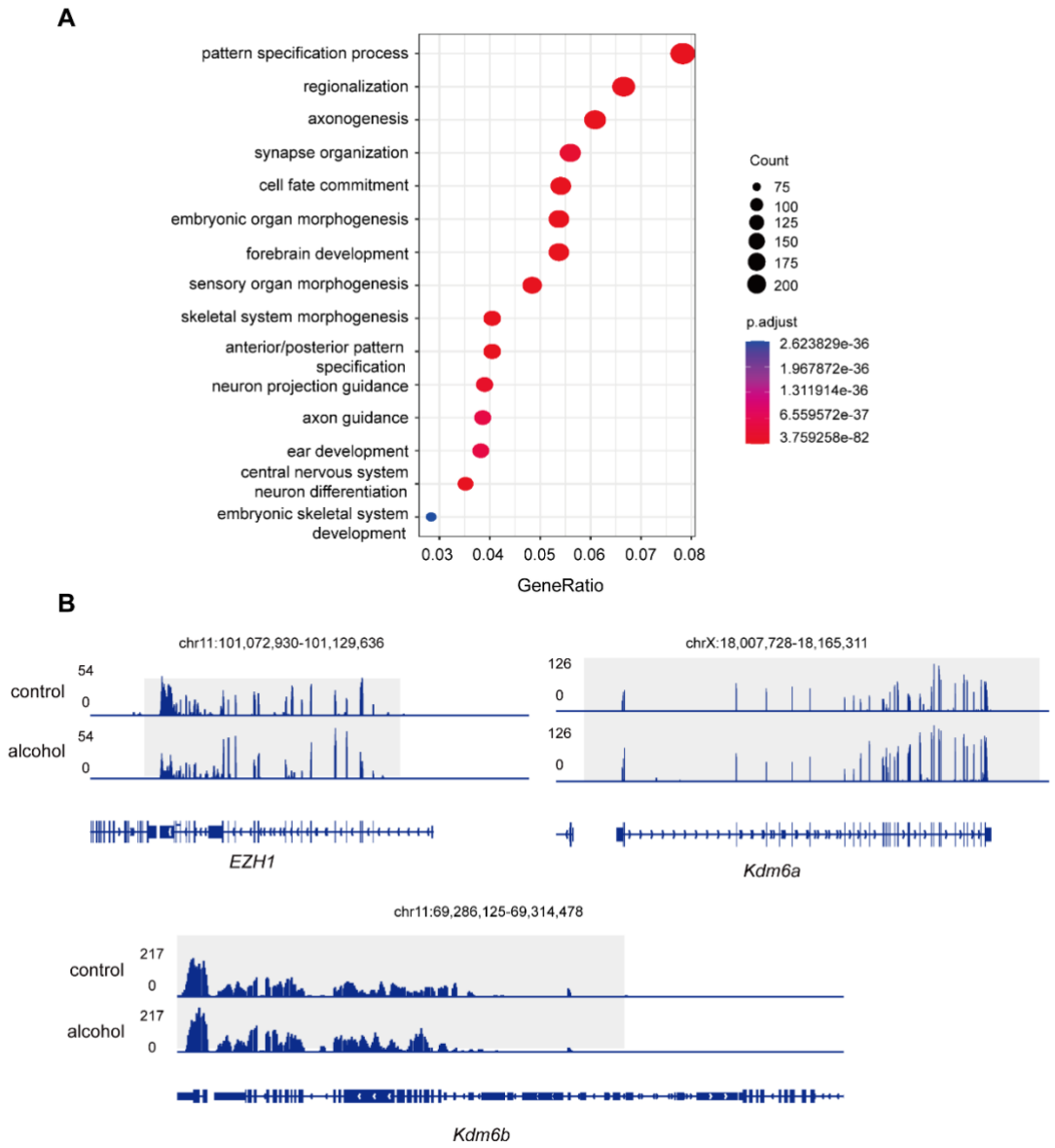

Figure S3. Alcohol exposure affects H3K27me3 establishment at development regulator genes without affecting the expression of H3K27me3 regulators. Related to Figure 2.

(A) Highly enriched GO biological processes of genes with impaired H3K27me3 deposition in alcohol-exposed Epiblasts, using R package clusterProfiler. (B) The IGV view of the expression levels of *Ezh1* (upper left), *Kdm6a* (upper right) and *Kdm6b* (below) in control and alcohol-exposed Epiblasts. Signals represent FPKM.

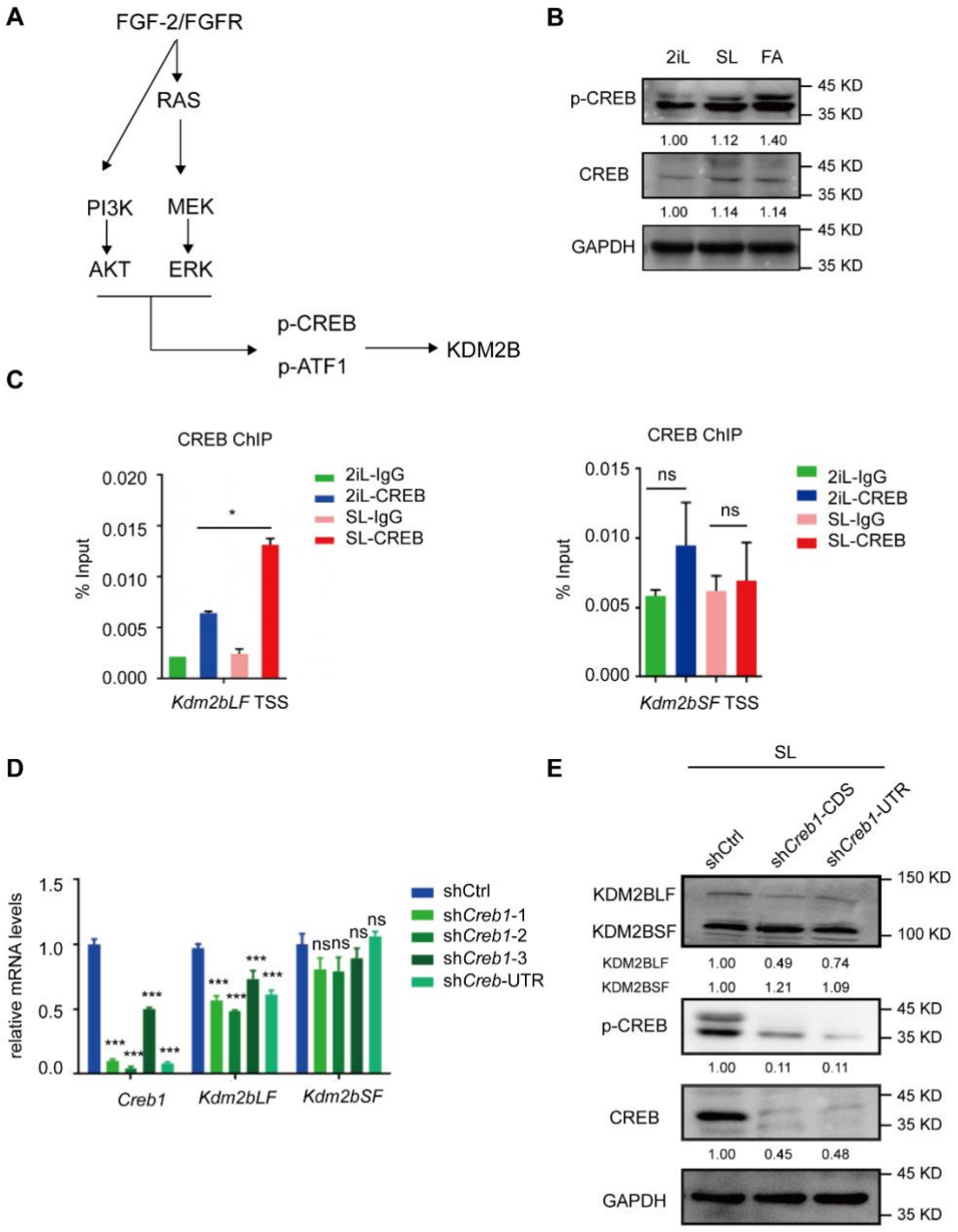
A
FGF-2/FGFR
RAS
PI3K
MEK
AKT
ERK
p-CREB
p-ATF1
KDM2B
B
2iL
SL
FA
p-CREB
45 KD
35 KD
1.00
1.12
1.40
CREB
45 KD
35 KD
1.00
1.14
1.14
GAPDH
45 KD
35 KD
C
CREB ChIP
% Input
0.020
0.015
0.010
0.005
0.000
*
2iL-IgG
2iL-CREB
SL-IgG
SL-CREB
Kdm2bLF TSS
CREB ChIP
% Input
0.015
0.010
0.005
0.000
ns
ns
2iL-IgG
2iL-CREB
SL-IgG
SL-CREB
Kdm2bSF TSS
D
relative mRNA levels
1.5
1.0
0.5
0.0
***
***
***
***
***
***
***
***
nsns
ns
ns
shCtrl
shCreb1-1
shCreb1-2
shCreb1-3
shCreb-UTR
Creb1
Kdm2bLF
Kdm2bSF
E
SL
shCtrl
shCreb1-CDS
shCreb1-UTR
KDM2BLF
KDM2BSF
150 KD
100 KD
KDM2BLF
1.00
0.49
0.74
KDM2BSF
1.00
1.21
1.09
p-CREB
45 KD
35 KD
1.00
0.11
0.11
CREB
45 KD
35 KD
1.00
0.45
0.48
GAPDH
45 KD
35 KD

Figure S4. Increased CREB activity is critical for the induction of KDM2BLF expression. Related to Figure 3.

(**A**) Pattern diagram showing FGF2-CREB signaling pathway for KDM2B activation. (**B**) WB analysis comparing total and phosphorylated CREB levels in 2iL, SL or FA-mESCs. GAPDH serves as loading controls. (**C**) ChIP-qPCR analysis showing the enrichment of CREB at the TSS of *Kdm2 LF* in mESCs in 2i or SL conditions. (**D**) RT-qPCR analysis showing the knockdown efficiency of *Creb1*. (**C**-**D**) Data are represented as means ± SEM. Two-tailed unpaired *t* test. *** *P*-value < 0.001; n.s. nonsignificant. (**E**) WB analysis comparing the expression levels of KDM2BLF and KDM2BSF, total and phosphorylated CREB levels in the control and CREB1 knockdown cells cultured under SL conditions. GAPDH serves as the loading control.

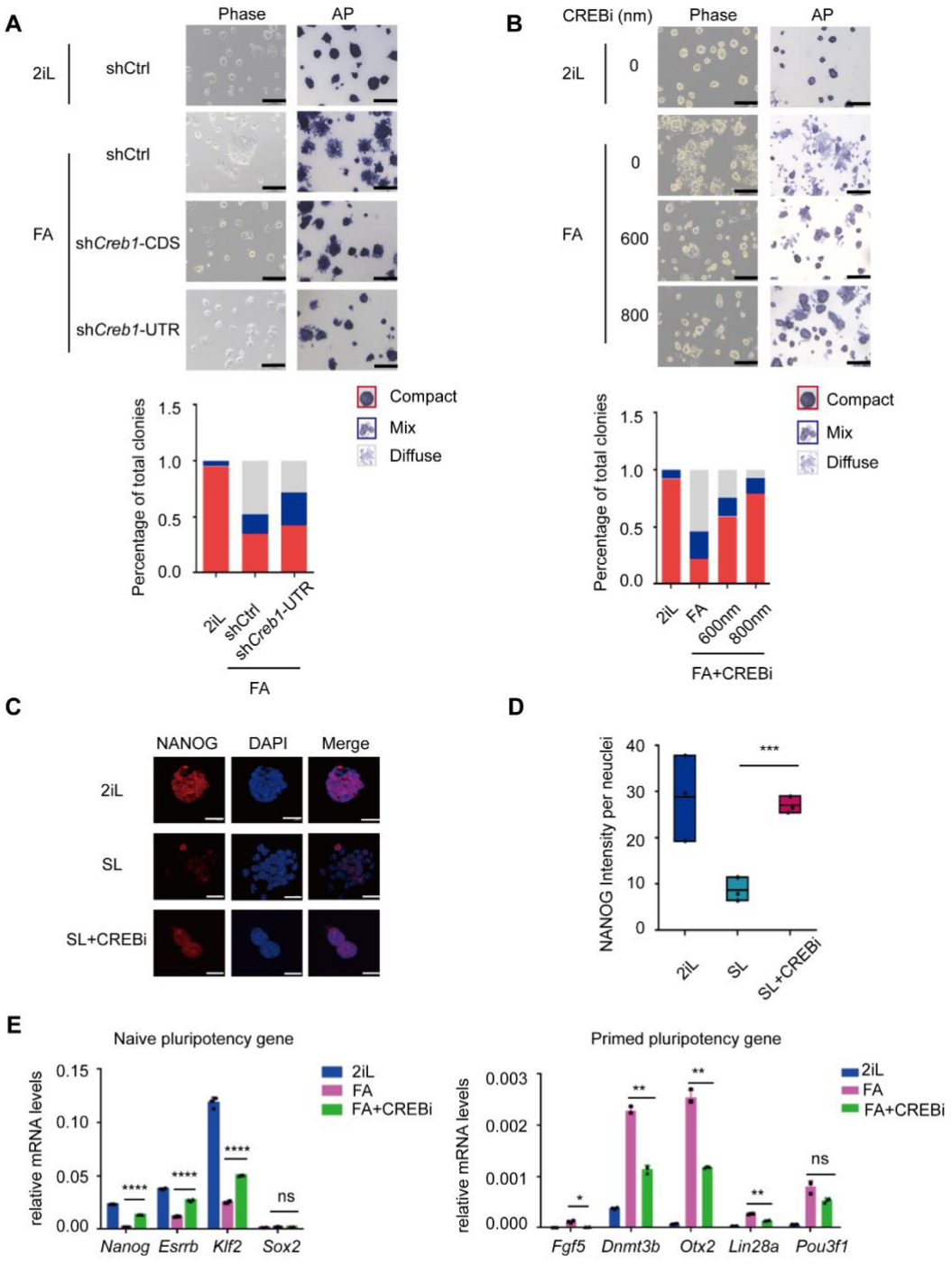
A
Phase
AP
2iL
shCtrl
FA
shCtrl
shCreb1-CDS
shCreb1-UTR
Compact
Mix
Diffuse
Percentage of total clonies
1.5
1.0
0.5
0.0
2iL
shCtrl
shCreb1-UTR
FA
B
CREBi (nm)
Phase
AP
2iL
0
FA
0
600
800
Compact
Mix
Diffuse
Percentage of total clonies
2iL
FA
600nm
800nm
FA+CREBi
C
NANOG
DAPI
Merge
2iL
SL
SL+CREBi
D
NANOG Intensity per neuclei
40
30
20
10
0
***
2iL
SL
SL+CREBi
E
Naive pluripotency gene
relative mRNA levels
0.15
0.10
0.05
0.00
2iL
FA
FA+CREBi
****
****
****
ns
Nanog
Esrrb
Klf2
Sox2
Primed pluripotency gene
relative mRNA levels
0.003
0.002
0.001
0.000
2iL
FA
FA+CREBi
*
**
**
**
ns
Fgf5
Dnmt3b
Otx2
Lin28a
Pou3f1

Figure S5. CREB activity is critical for exit from naïve pluripotency. Related to Figure 3.

(**A-B**) Comparison of morphology and AP staining between the control and *Creb1* knockdown mESCs (**A**), and among 2iL, FA or FA+CREBi-mESCs (**B**). Bottom for (**A-B**): quantitative morphology (compact, mixed, diffuse) analysis, gray represents diffuse, blue represents mixed, and red represents compact. Scale bars, 100 μm. (**C**) IF analysis of NANOG expression levels in 2iL, FA or FA+CREBi-mESCs. Scale bars, 100 μm. (**D**) Statistical analysis of NANOG expression levels using cellprofiler software. (**E**) RT-qPCR analysis of naïve (left) and primed pluripotency (right) gene in 2iL, FA or FA+CREBi-mESCs. Two-tailed unpaired *t* test for (**D-E**). Data are represented as means ± SEM. *** $P < 0.001$, ** $P < 0.01$, n.s. nonsignificant.

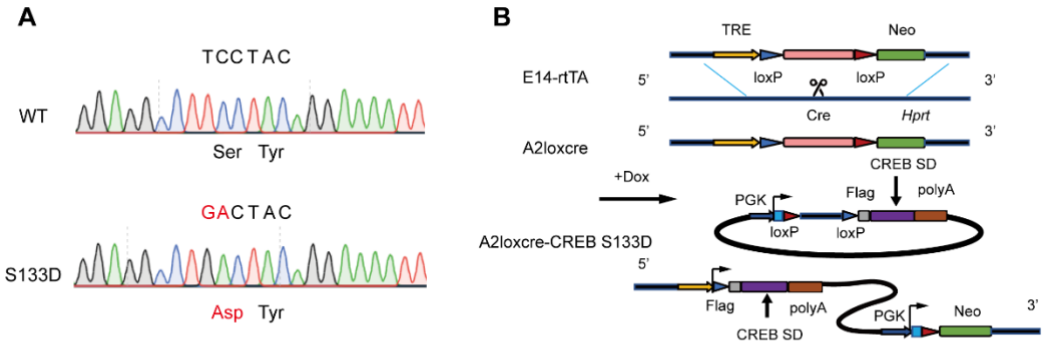

Figure S6. Construction of the icaCREB ESC line. Related to Figure 3.

(**A**) Schematic diagram shows the locus of S133D of CREB. (**B**) Schematic of construction of DOX-inducible expression of FLAG-CREBS133D (the constitutively activation form of CREB) in mESCs.

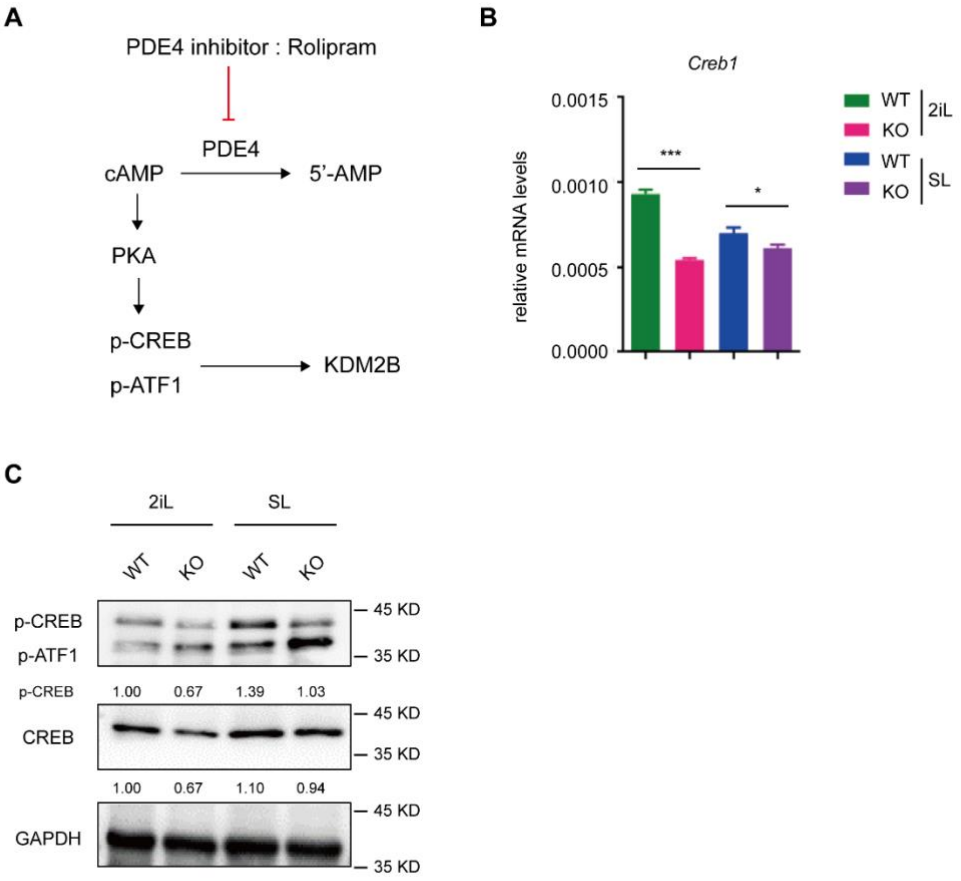

Figure S7. Potential functional interplay between CREB and KDM2B. Related to Figure 4.

(**A**) The signaling pathway diagram of PDE4 inhibitor Rolipram activating CREB/KDM2B axis. (**B**) RT-qPCR analysis of Creb1 expression levels in WT and *Kdm2bLF*-KO mESCs cultured under indicated conditions. Data are represented as means ± SEM. Two-tailed unpaired *t* test. n=3, *, $P<0.05$; ***, $P < 0.001$. (**C**)WB analysis of CREB and p-CREB levels in WT and *Kdm2bLF*-KO mESCs cultured under indicated conditions. GAPDH serves as the loading control.

Table S4. List of oligonucleotides.

Use	Primer name	Sequence 5'-3'
qPCR	*Creb1*-qPCR-F	TGCCAACCCCCATTTACCAA
	Creb1-qPCR-R	TGTCCATCAGTGGTCTGTGC
	Kdm2bLF-qPCR-F	GTTTCACTGACTTCCACATTGACTTT
	Kdm2bLF-qPCR-R	GCAGGGTTGGAGGGATCAG
	Kdm2bSF-qPCR-F	CCGAGGACGACGACTATGAATC
	Kdm2bSF-qPCR-R	ACCTCCAAACTTCTTCATGTCCTT
	Nanog-qPCR-F	GCTTTGAAGCATCCGACTGTA
	Nanog-qPCR-R	TCTTGACCGGGACCTTGTCT
	Esrrb-qPCR-F	TACCTGAACCTGCCGATTTC
	Esrrb-qPCR-R	CCCAGTTGATGAGGAACACA
	Klf2-qPCR-F	TACACCAACTGCGGCAAGAC
	Klf2-qPCR-R	CGCACAAGTGGCACTGAAAG
	Sox2-qPCR-F	GCGGAGTGGAAACTTTTGTCC
	Sox2-qPCR-R	GGGAAGCGTGTACTTATCCTTCT
	Fgf5-qPCR-F	AGCGCGACGTTTTCTTCGT
	Fgf5-qPCR-R	GCCATTGACTTTGCCATCCG
	Dnmt3b-qPCR-F	GCTATTTGTCTTGAGGCGCT
	Dnmt3b-qPCR-R	AACTTAGAACCCAGGAGACGC
	Otx2-qPCR-F	GGAGAGGACGACATTTACTAGG
	Otx2-qPCR-R	TTCTGACCTCCATTCTGCTG
	Pou3f1-qPCR-F	TTTGTATGCCCGACTAAACC
	Pou3f1-qPCR-R	ACAGATGAAGAAATGGTGAAGG
	Lin28a-qPCR-F	GTTCGGCTTCCTGTCTATGACC
	Lin28a-qPCR-R	CTTCCATGTGCAGCTTGCTCT
	Klf4-qPCR-F	GTGCCCCGACTAACCGTTG
	Klf4-qPCR-R	GTCGTTGAACTCCTCGGTCT
ChIP-qPCR primer	*Hoxb9*-ChIP-F	CCATCCTGGATATGGAATGC
	Hoxb9-ChIP-R	GGAGCTCCTTGCAAAATGAT
	Fgf3-ChIP-F	CAGATCAGGCCCATCCCG
	Fgf3-ChIP-R	GCGTGTGCTCCCAGCG
	Sox2-ChIP-F	TCATGCAAAACCCTCTGGCG
	Sox2-ChIP-R	GGAATAAATGGGTTTCCGGC
	Wnt1-ChIP-F	TGCGCCCTGGTGCTTTTAGTGC
	Wnt1-ChIP-R	GCGGGCCGCAGGCAGCATG
shRNA	sh*Creb1*-1	AACCAGCAGAGTGGAGATGCT
	sh*Creb1*-2	AAGTCAGAAGAGGAGACTTCA
	sh*Creb1*-3	CAGCAGCTCATGCAACATCAT
	sh*Creb1*-UTR	GCCTGAAAGCAACTACAGAAT
Creb1 mRNA	PCR8-m*Creb1*-F	AAAAAAGCAGGCTCCGAATTC atgaccatggaatctggagca

generation	PCR8-m*Creb1*-R	CAAGAAAGCTGGGTCGAATTC ttaatctgatttgtggcagt
Creb1S133D mRNA generation	m*Creb1* S133Dmut-F	AGGCCTGACTACAGGAAAAT TTTGAATGACTTATCTTC
	m*Creb1* S133Dmut-R	TTCCTGTAGTCAGGCCTC CTTGAAAGGATTTCC
KDM2B LF KO	*Kdm2bLF*-sgRNA-1	CACC AAACGGATCTGCTTAAGTGT
	Kdm2bLF-sgRNA-2	CACC CATTTTCAGCAGTTGTGGGG